

Numerical study of some flow and heat transfer problems involving generalized Newtonian fluid



Research thesis submitted in the partial fulfillment for the

Degree of Master of Science in Mathematics

by

Aiman Sultan

Supervised by

Dr. Meraj Mustafa Hashmi

School of Natural Sciences (SNS),
National University of Sciences and Technology (NUST),
Islamabad, Pakistan

2016 - 2018




National University of Sciences & Technology

MASTER'S THESIS WORK

We hereby recommend that the dissertation prepared under our supervision by: Ms. Aiman Sultan, Regn No. 00000106747 Titled: Numerical study of some flow and heat transfer problems involving generalized Newtonian fluids be accepted in partial fulfillment of the requirements for the award of **MS** degree.

Examination Committee Members

1. Name: DR. MUJEEB UR REHMAN Signature: 

2. Name: DR. M. ASIF FAROOQ Signature: 

External Examiner: PROF. MUHAMMAD AYUB Signature: 

Supervisor's Name DR. MERAJ MUSTAFA HASHMI Signature: 


Head of Department

16/08/18
Date


COUNTERSIGNED


Date: 16/08/18

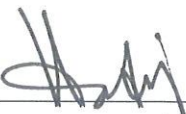

Dean/Principal

THESIS ACCEPTANCE CERTIFICATE

Certified that final copy of MS thesis written by Ms. Aiman Sultan (Registration No. 00000106747), of School of Natural Sciences has been vetted by undersigned, found complete in all respects as per NUST statutes/regulations, is free of plagiarism, errors, and mistakes and is accepted as partial fulfillment for award of MS/M.Phil degree. It is further certified that necessary amendments as pointed out by GEC members and external examiner of the scholar have also been incorporated in the said thesis.

Signature: 
Name of Supervisor: Dr. Meraj Mustafa Hashmi
Date: 16/08/18

Signature (HoD): 
Date: 16/08/18

Signature (Dean/Principal): 
Date: 16/08/18

I DEDICATE THIS THESIS TO MY FAMILY

ACKNOWLEDGEMENT

Praise be to ALLAH, the Almighty for the blessing and mercy, health and inspirations that had been given to me for completion of my MS successfully.

Darood and Salaam always dedicated to our beloved Prophet MUHAMMAD (SAWW), the last prophet, the prophet who had brought us from the darkness to the lightness. Best prayers and peace be unto his pure descendant, and his family and his noble companions.

I would like to extend my gratitude to my Parents and siblings for their unfailing support and encouragement throughout my study years and during research and thesis writing. This accomplishment would not have been done without them.

I would like to show my gratitude to my husband for his support and inspiring suggestions. His useful feedback and insightful comments on my work always helped me.

I would like to acknowledge National University of Sciences and technology (NUST) for giving me admission in MS Mathematics and providing the peaceful environment for my studies.

I would like to acknowledge Dr. Habib Nasir principal SNS, NUST for providing the peaceful environment and all the possible research facilities.

I would like to thank my supervisor Dr. Meraj Mustafa Hashmi for providing me the opportunity of taking part in this research project. I am grateful for his help, guidance and support throughout the research and my entire course work, I am short of words to express my deep and sincere appreciation towards his dedicated hard work,

I would like to thank my GEC members Dr. Mujeeb ur Rehman and Dr. Asif Farooq for their kind attitude and endless support.

I would like to show my gratitude to Dr. Muhammad Ayub (External Supervisor) for his support and inspiring suggestions.

I would like to extend my heartiest gratitude to my lovely, worthy and the friendliest classmates at NUST. They were fundamental in supporting me during this time period. My coursework and research would not have been possible without them. I would like to mention the names: Amna Sadiq, Aqsa Marrium, Maria Tabassum, Razia Sharif, Sadaf Khan and Shawana Khan.

AIMAN SULTAN

Contents

1	Introduction	1
1.1	Basic definitions and preliminaries.....	1
1.1.1	Newtonian fluids.....	1
1.1.2	Non-Newtonian fluids.....	1
1.1.3	Shear thinning and shear thickening fluids.....	2
1.1.4	Steady and unsteady flows.....	2
1.1.5	Compressible and incompressible flows.....	2
1.1.6	Laminar and turbulent flows.....	3
1.1.7	Boundary layer.....	3
1.1.8	Stagnation-point.....	3
1.1.9	Cross fluid model	3
1.2	Some dimensionless numbers	
1.2.1	Reynolds number.....	4
1.2.2	Prandtl number.....	4
1.2.3	Weissenberg number.....	4
1.2.4	Schmidt number.....	5
1.3	Boundary layer equations governing MHD flow of Cross fluid.....	5
1.4	Equation of heat transfer with variable thermal conductivity.....	6
1.5	Equation of mass transfer.....	6
1.6	Literature review.....	7
1.7	Numerical methods.....	10
1.7.1	Shooting technique.....	10
1.7.2	bvp4c.....	11
2	Aiding or opposing MHD flow of generalized Newtonian fluid along a non-isothermal surface with variable thermal conductivity	12
2.1	Problem formulation.....	12
2.2	Numerical results and discussion.....	16
2.3	Concluding remarks.....	24

3 Pressure driven flow of Cross fluid along a stationary plate subject to binary chemical reaction and Arrhenius activation energy	26
3.1 Problem formulation.....	26
3.2 Method of solution.....	29
3.3 Results and discussion.....	30
3.4 Concluding remarks.....	36
References.....	38

Preface

Fluids in which shear stress and deformation rate are not linearly related to each other are termed as non-Newtonian fluids. Mining industries, chemical and plastic processing industries, lubrications and polymer industries usually involve non-Newtonian fluid flows. Non-Newtonian fluids may be categorized as shear thinning and shear thickening fluids. The apparent viscosity of shear-thickening (dilatant) fluids increase on increasing shear rate. Whereas fluids for which apparent viscosity reduces on increasing shear rate are known as shear-thinning (pseudoplastic) fluids.

Viscosity of fluids like blood, paints and detergents decrease as shear rate is increased and are regarded as shear thinning fluids. Cross and Carreau models are significant as they reflect the viscosity and fluid behavior at both low and high shear rates. Cross fluid is a category of generalized Newtonian fluids whose apparent viscosity is a function of deformation rate.

Chapter 1 includes some relevant definitions, boundary layer equations, comprehensive literature review concerning the problems discussed and the method that is being used to obtain significant results throughout.

Cross rheological fluid under different circumstances has been analyzed in this thesis. Chapter 2 deals with two-dimensional MHD stagnation point flow of Cross fluid towards a vertical stretchable surface. Variable wall temperature and variable thermal conductivity are assumed in the problem. The governing equations are transformed by means of usual similarity transformation method. Numerical results obtained through `bvp4c` and shooting method both match really well with each other. Comparison of our calculations with that of already published one clearly illustrate the authenticity of our code. The impact of various important parameters on flow and heat transfer are presented through various graphs.

Chapter 3 is concerned with the flow of Cross rheological fluid over a stationary rigid plate heated by a heat source. The presence of magnetic field has impact on the behavior of fluid flow. Fluid is assumed to have variable thermal conductivity. Mass equation is modeled in terms of activation energy and chemical reaction. Governing equations are transformed by adopting the

similarity transformation mechanism. Bvp4c is used to obtain numerical results. The graphs plotted reveal the physical influence of significant parameters on fluid properties.

Chapter 1

Introduction

This chapter is concerned with some of the basic definitions and preliminaries. Boundary layer equations governing flow, heat and mass transfer of Cross fluid have also been discussed in this chapter.

1.1 Basic definitions and preliminaries

1.1.1 Newtonian fluids

Fluids that obey Newton's law of viscosity are categorized as Newtonian fluids. Mathematically, Newton's law of viscosity can be expressed as

$$\tau_{xy} = \mu \frac{du}{dy} \quad (1.1)$$

where τ_{xy} is the shear stress, du/dy is the deformation rate and μ is the dynamic viscosity of the fluid. Air, water and oil are some of the common examples of Newtonian fluids.

1.1.2 Non-Newtonian fluids

Fluids in which shear stress and deformation rate are not linearly related to each other are termed as non-Newtonian fluids. Such fluids may be described by the power-law model given below:

$$\tau_{xy} = K \left(\frac{du}{dy} \right)^n \quad (1.2)$$

in which K is the consistency index and n represents the flow behavior index.

Eq. (1.2) can be written in the form

$$\tau_{xy} = \eta \frac{du}{dy} \quad (1.3)$$

in which $\eta = K \left(\frac{du}{dy} \right)^{n-1}$ is the apparent viscosity.

1.1.3 Shear-thinning and shear-thickening fluids

Fluids for which apparent viscosity reduces upon increasing shear-rate are termed as shear-thinning. Blood and paints are commonly encountered shear-thinning fluids. On the other hand the apparent viscosity of shear-thickening (dilatant) fluids increases with increasing shear rate. Quick sand and plant resin are examples of dilatant fluids.

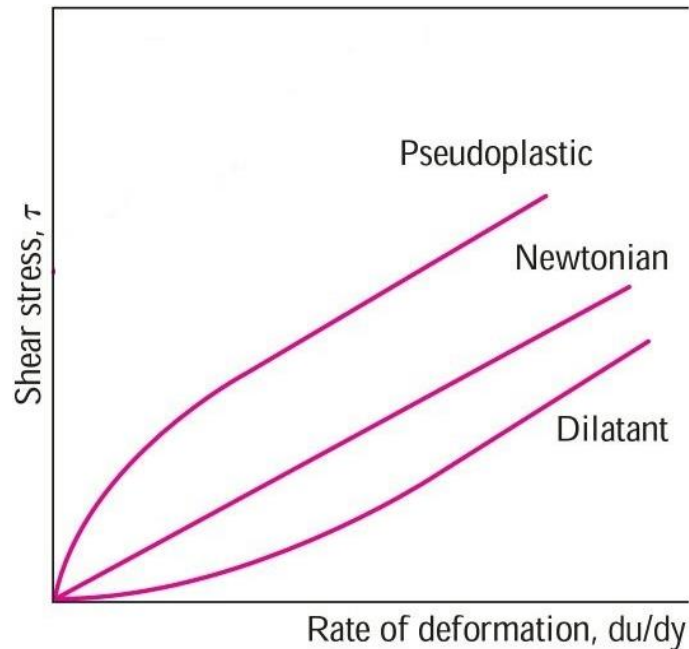


Fig 1.1: Behavior of shear-thinning (pseudoplastic) and shear-thickening (dilatant) fluids.

1.1.4 Steady and unsteady flows

The flow in which fluid properties such as velocity, temperature, density and pressure are time-independent at everywhere in the flow field is known as steady flow. In unsteady flow, fluid properties are time-dependent, i.e., they vary as the time progresses.

1.1.5 Compressible and incompressible flows

Flow in which fluid density changes due to variation in pressure is known as compressible flow. In aerodynamics, fluids with Mach greater than 0.3 are assumed to be compressible. On the other

hand, for incompressible fluids, density does not vary across the flow field. Most of the liquids are incompressible having Mach less than 0.3.

1.1.6 Laminar and turbulent flows

Flow that occurs in parallel layers is known as laminar flow. While in the case of turbulent flow, adjacent layers flow in an irregular pattern and cause disruption in the motion.

1.1.7 Boundary layer

Solid surface and the fluid in contact with it attain almost equal velocity. This velocity gradually varies from layer to layer. The layer of fluid that approaches free stream is known as boundary layer. Within the boundary layer, the effect of frictional force is prominent. Free stream velocity is maintained outside the boundary layer.

1.1.8 Stagnation-point

Stagnation point refers to that point in the flow field at which fluid experiences zero local velocity.

1.1.9 Cross fluid model

Cross [1] proposed the following relationship between apparent viscosity η and shear rate $\dot{\gamma}$ for shear-thinning fluids:

$$\frac{\eta - \eta_{\infty}}{\eta_0 - \eta_{\infty}} = \left(\frac{1}{1 + (K|\dot{\gamma}|)^n} \right). \quad (1.4)$$

In the above equation, η_0 denotes the viscosity at zero shear rate. η_{∞} stands for infinite shear rate viscosity which is appropriate in predicting material's response in case of high shearing situations. K is the consistency index or Cross time constant. Here $1/K$ is the critical shear rate which indicates the commencement of shear rate. Flow behavior index n , a dimensionless number, measures the dependence of viscosity on deformation rate in the shear-thinning region.

1.2 Some dimensionless numbers

1.2.1 Reynolds number

Reynolds numbers (Re) is a dimensionless number, that is used to classify laminar and turbulent flow situations. Mathematically, it measures the ratio of inertial force to viscous force. That is,

$$Re = \frac{\rho v L}{\mu} = \frac{v L}{\nu} \quad (1.5)$$

where L is the characteristic length. At low Reynolds number, viscous force dominates inertial force, which in turn results into laminar flow. Whereas, inertial force becomes relatively dominant at high Reynolds number producing turbulence in the fluid flow.

1.2.2 Prandtl number

Prandtl number (Pr), named after its inventor Ludwig Prandtl, is a dimensionless number that is used to calculate heat transfer between a solid surface and a moving fluid. In mathematical terms, it represents the ratio of kinematic viscosity to the thermal diffusivity:

$$Pr = \frac{\nu}{\alpha} = \frac{c_p \mu}{k}, \quad (1.6)$$

where $\nu = \mu/\rho$ denotes the kinematic viscosity, $\alpha = k/\rho c_p$ stands for thermal diffusivity of the fluid in which k represents thermal conductivity and c_p stands for specific heat capacity.

1.2.3 Weissenberg number

As the deformation rate is reduced to zero, material relaxes over its characteristic relaxation time, known as stress relaxation.

Weissenberg number (We) is a dimensionless number, defined as the product of shear rate and relaxation time of the fluid.

1.2.4 Schmidt number

Schmidt number (Sc) gives the ratio of kinematic viscosity to the mass diffusivity. Mathematically,

$$Sc = \frac{\nu}{D}, \quad (1.8)$$

where D stands for mass diffusivity.

1.3 Boundary layer equations governing MHD flow of Cross fluid

Relevant equations governing the unsteady laminar and incompressible flow are:

$$\nabla \cdot \mathbf{V} = 0, \quad (1.9)$$

$$\rho \left(\frac{\partial \mathbf{V}}{\partial t} + (\mathbf{V} \cdot \nabla) \mathbf{V} \right) = -\nabla p + \nabla \cdot \mathbf{S} + (\mathbf{J} \times \mathbf{B}), \quad (1.10)$$

where $\mathbf{V} = (u(x, y), v(x, y), 0)$ denotes the Cartesian velocity field, \mathbf{J} is the current density and \mathbf{B} is the magnetic flux density. $\mathbf{S} = 2\eta\mathbf{D}$ is the extra stress tensor in which $\mathbf{D} = [(\nabla\mathbf{V}) + (\nabla\mathbf{V})^t]/2$ represents the deformation rate tensor and η is the apparent viscosity of Cross fluid as in Eq. (1.4). Assuming infinite shear rate viscosity to be zero, we get:

$$\mathbf{S} = \left(\frac{\eta_0}{1 + (K|\dot{\gamma}|)^n} \right) [(\nabla\mathbf{V}) + (\nabla\mathbf{V})^t]. \quad (1.11)$$

Here

$$\dot{\gamma} = (2D_{kl}D_{kl})^{1/2} = \left(4 \left(\frac{\partial u}{\partial x} \right)^2 + \left(\frac{\partial u}{\partial y} + \frac{\partial v}{\partial x} \right)^2 \right)^{1/2} \quad (1.12)$$

is the shear rate.

The current density \mathbf{J} can be expressed as:

$$\mathbf{J} = \sigma(\mathbf{E} + \mathbf{V} \times \mathbf{B}), \quad (1.13)$$

in which σ represents the fluid electrical conductivity and \mathbf{E} is the electric field that is assumed to be absent.

Thus we get,

$$\mathbf{J} \times \mathbf{B} = (-\sigma B^2 u, 0, 0). \quad (1.14)$$

Using (1.9), (1.10) and then applying boundary layer approximations, we arrive at the following:

$$\frac{\partial u}{\partial x} + \frac{\partial v}{\partial y} = 0, \quad (1.15)$$

$$uu_x + vu_y = -\frac{1}{\rho} p_x + \nu \left[\frac{\partial}{\partial y} \left(\frac{u_y}{1 + (K|\dot{\gamma}|)^n} \right) \right] - \frac{\sigma B^2}{\rho} u. \quad (1.16)$$

where u and v are the respective x and y directional velocity components.

1.4 Equation of heat transfer with variable thermal conductivity

In absence of viscous dissipation and heat generation, equation governing the law of conservation of energy is:

$$\rho c_p \left(\frac{\partial T}{\partial t} + (\mathbf{V} \cdot \nabla) T \right) = -\nabla \cdot \mathbf{q}, \quad (1.19)$$

in which c_p is the specific heat capacity and $\mathbf{q} = -(k(T))(\partial T/\partial y)$ is the heat flux. Therefore under boundary layer approximations, Eq. (1.19) attains following form:

$$\rho c_p \left(u \frac{\partial T}{\partial x} + v \frac{\partial T}{\partial y} \right) = \frac{\partial}{\partial y} \left(k(T) \frac{\partial T}{\partial y} \right), \quad (1.20)$$

with $k(T) = k_\infty(1 + \epsilon(T - T_\infty)/\Delta T)$ in which k_∞ is the thermal conductivity at the ambient, T_∞ is the fluid temperature at the ambient and $\epsilon > 0$ is a constant.

1.5 Equation of mass transfer

The relevant equation describing the mass transfer phenomenon in the presence of activation energy E_a is expressed as:

$$\mathbf{V} \cdot \nabla C = \nabla \cdot D \nabla C - k_r^2 \left(\frac{T}{T_\infty} \right)^m e^{\frac{-E_a}{\kappa T}} (C - C_\infty), \quad (1.21)$$

where C denotes the solute concentration, D is the mass diffusivity. Modified Arrhenius function is represented by the term $k_r^2 \left(\frac{T}{T_\infty}\right)^m e^{\frac{-E_a}{\kappa T}}$ in which k_r^2 represents the reaction rate, m denotes the fitted rate constant and lies in $-1 < m < 1$ while $\kappa = 8.61 \times 10^{-5} \text{eV/K}$ represents the Boltzmann constant.

After the use of boundary layer approximations, Eq. (1.21) becomes:

$$\left(u \frac{\partial C}{\partial x} + v \frac{\partial C}{\partial y}\right) = D \frac{\partial^2 C}{\partial y^2} - k_r^2 \left(\frac{T}{T_\infty}\right)^m e^{\frac{-E_a}{\kappa T}} (C - C_\infty). \quad (1.22)$$

1.6 Literature review

The viscosity of most liquids we encounter in real world applications is independent of the applied external force. But there exists a large class of substances for which mechanical properties deviate from Newtonian constitutive relation to a greater or lesser extent. Nearly all polymer melts, polymer solutions, biological fluids, mayonnaise, sand in water etc. exhibit shear thinning behavior; that is, the viscosity function of such fluids reduce with increasing shear rate. For relatively small group of fluids, the apparent viscosity is proportional to the shearing force. Such fluids are termed as shear- thickening or dilatant (expanding) fluids. The well-known power law (or Ostwald-de-Waele) model [2,3] offers simplest representation of shear-thinning/thickening flow behavior in many fluids including polymeric solutions and melts, dispersions and weak gels. However this model is applicable for only a limited range of shear rates. Also it does not predict flow behavior for zero and infinite shear viscosities. In such cases, one must resort to four parameter Cross [1] and Carreau [4] rheological models. These models have been found appropriate in predicting shear-thinning effects for both low and high shear rates. Fluid model due to Cross [3] is a four parameter model that is adequate in flow description of many pseudoplastic liquids even in the regions of low and high shear rates. Xie and Jin [4] conducted a parametric study of Cross rheological model and applied it to analyze a specific non-Newtonian flow problem using computational approach. Khan et al. [5] modeled effect of activation energy on flow of shear-thinning fluid in the region of stagnation-point utilizing Cross rheological equation. Cross rheological equation for fluid flow along a stretching plate with heat transfer was recently examined by Khan et al. [6]. Such problem for the axisymmetric case was

resolved in another paper by Khan et al. [7]. Very recently, the onset of activation energy for stagnation-point flow of Cross fluid was numerically elucidated by Khan et al. [8].

A huge number of explorations dealing with stagnation flows around stretchable surfaces are taking place due to their enormous applications in manufacturing processes including paper production, manufacturing of glass and fiber, crystal growth process, food and polymer processing, plasma studies and aerodynamics to name a few. In such applications, cooling rate of stretching surface is vital which is directed by the structure of thermal boundary layer near the strip. Particularly, stagnation-point flows play an important role in measuring drag coefficient within stagnation regions of objects immersed in rapidly moving fluids. Decades ago, Heimenz [9] discovered an exact solution for two-dimensional stagnation-point flow striking normal to an infinite flat plate. Homann [10] extended this concept for the axisymmetric case. Heimenz's work has led to many subsequent research articles in this direction in which Chiam [11] considered the stagnation-point flow developed over an elastic sheet expanding linearly in its own plane. He observed that flow near the surface is similar to the external flow resulting in no boundary layer formation. Heat transfer to fluid flow in the vicinity of stagnation-point on a continuously deforming sheet was examined by Mahapatra and Gupta [12]. An extension to this problem was made by Ishak et al. [13] for buoyancy effects arising due to fluid flow along a vertical surface. Wang [14] found a novel exact solution for axisymmetric stagnation-point flow of rarefied gases subject to first-order wall slip. Viscoelastic effects in stagnation-point flow near stretchable surface were elucidated by Mahapatra et al. [15] through second-grade rheological model. Mahapatra et al. [16] obtained similarity solution for MHD power-law fluid flow near a stagnation-point towards an extensible surface. The shear-thinning/thickening behavior of power-law fluid was addressed. This problem was later solved by Mahapatra et al. [17] for wide-ranging values of magnetic interaction parameter using homotopic approach. Stagnation-point flow problem for micropolar fluid was also attempted in a paper by Nazar et al. [18]. Bachok et al. [19] discussed the onset of heat conduction in stagnation flow due to melting of stretchable surface. A few recent contributions in the area were published by Mushtaq et al. [20], Mustafa et al. [21], Shen et al. [22], Mustafa et al. [23], Naganthran et al. [24] and Mansur et al. [25].

MHD character of fluid is particularly important in many technical applications including design of power generations, magnetic separation, blood flow and blood pump machines, targeted

transport of drugs using ferromagnetic particles as drug carriers etc. Due to this reason, a considerable number of research work concerning the application of magnetic field in boundary layer flows have been appeared in recent past (see refs. [26]-[31] and studies there in.).

Modeling transfer of heat and chemically reactive substances in fluid flow has essence in wide-ranging processes in chemical industries including condensation, vaporization, diffusion, alcohol distillation, gas absorption and applications in oil reservoirs, nuclear reactor cooling and much more. In particular, temperature dependent reaction rate becomes important in processes involving geothermal and oil reservoir engineering and in understanding the dynamics of water and oil emulsions. In recent years, vast wealth of material concerning fluid flow comprising chemically reactive substances is published. For example, Maxwell fluid flow along a stretchable surface comprising reactive nanoparticles was examined by Afify and Elgazery [32] using a numerical approach. Chemical reaction with double diffusion in a power-law fluid flow through a spongy/permeable space was considered by Zhuang et al. [33]. A numerical study describing the flow of non-Newtonian Sisko fluid near a cylindrical surface influenced by chemical reaction was conducted by Malik and Khan [34]. The effect of chemically reacting solute on unsteady non-Newtonian fluid between a squeezing channel was investigated by Adesanya et al. [35]. Hayat et al. [36] analytically examined chemical reaction effects on MHD flow between rotating porous disks. Similar attempts in this domain can be pursued through [37]-[41] and refs. there in.

Activation energy is the least obligatory amount of energy for chemical system with potential reactants to experience a chemical reaction. The source of activation energy required to initiate chemical reactions is typically heat energy from the surroundings. Bestman [42] analyzed natural convective flow of binary mixture along a moving permeable wall using a perturbation scheme. Maleque et al. [43] utilized modified Arrhenius function to model the onset of activation energy on MHD flow induced by a moving plate. In another study [44], they explored natural convection along a permeable surface with chemical reaction rate depending on activation energy. Awad et al. [45] explored activation energy aspects for unsteady flow of binary fluid in rotating frame. Later, Shafique et al. [46] also made use of Arrhenius function to model mass transport in binary viscoelastic fluid flow subject to rotating frame. Recently published reports in this domain can be found in refs. [47]-[50].

The purpose of this thesis is two fold. Firstly, we will analyze the stagnation-point flow impinging normal to a vertical stretchable surface placed in a generalized Newtonian fluid. Our interest is to elucidate the role of Cross rheology equation on the underlying physics of the problem. Moreover, the flow field accounts for the effects of magnetic field. Secondly, we intend to model the non-Newtonian flow along a rigid plate caused by stream-wise pressure gradient when Cross rheological equation is involved. In this work, variation in fluid thermal conductivity with absolute temperature is considered. Furthermore, the flow field is assumed to contain chemically reacting solute. Thus mass transfer process is formulated via modified Arrhenius function for activation energy.

1.7 Numerical Methods

1.7.1 Shooting technique

Consider the third order ODE:

$$y''' = f(x, y, y', y''), a \leq x \leq b, \quad (1.25)$$

subject to the boundary conditions:

$$y(a) = c_1, y'(a) = c_2, y(b) = c_3. \quad (1.26)$$

Here a, b, c_1, c_2 and c_3 are constants. By using the substitutions $y_1 = y, y_2 = y', y_3 = y''$, we aim to transform the ODE to a system of three first order ODEs given as:

$$y_1' = y_2, \quad (1.27)$$

$$y_2' = y_3, \quad (1.28)$$

$$y_3' = y''' = f(x, y_1, y_2, y_3), \quad (1.29)$$

subjected to the initial conditions:

$$y_1(a) = c_1, y_1'(a) = c_2, y_1''(a) = p. \quad (1.30)$$

In order to find c_3 we have to find p , such that solution at $x = b$ is satisfied. For this purpose we choose $p = p_q$ such that

$$\lim_{q \rightarrow \infty} y(b, p_q) = y(b) = c_3. \quad (1.31)$$

Now we generate a sequence p_1, p_2, p_3, \dots with p_0 as our initial guess such that the iteration stops when $y(b, p) - c_3 = 0$.

Fifth order Runge-Kutta (RK-5) method is employed in order to solve our first order ODEs along with the initial conditions (1.30).

The sequence p_1, p_2, \dots is generated by Newton-Raphson method illustrated as:

$$p_{n+1} = p_n - \frac{y(b, p_n) - c_3}{\frac{d}{dq}(y(b, p_n))}. \quad (1.32)$$

1.7.2 bvp4c

MATLAB routine bvp4c is a numerical technique that is capable of solving non-linear boundary value problems. To implement this technique, we first reduce third order ODE into first order ODEs. This code uses collocation method to obtain solutions to these ODEs over a particular domain. Changes are made in the step size to obtain accurate results. Ref. [51] and [52] are suggested for detail understanding.

Chapter 2

Assisting or opposing MHD flow of Cross fluid along a non-isothermal surface with variable thermal conductivity

This chapter includes detailed discussion of aiding or opposing MHD flow near stagnation-point on a vertical stretchable surface having variable wall temperature distribution. The surface is immersed in a generalized Newtonian fluid that obeys Cross rheology equation. Fluid under consideration has variable thermal conductivity. By choosing the usual transformations, the governing equations of fluid motion and energy transfer are changed into similar forms. Numerical computations are performed to study the influences of Cross fluid parameters on mean physical quantities. In particular, shear thinning character of Cross fluid is investigated from the obtained results.

2.1 Problem formulation

Consider a two-dimensional stagnation-point flow of Cross fluid impinging normal to an infinite plane wall aligned with $y = 0$. It is assumed that wall stretches, that is, expands in the x -direction with rate c_1 . The external flow is characterized by $u_e(x) = c_2x$ and $v_e(y) = -c_2y$, where $c_2 > 0$ is a constant (see Fig. 2.1). Transverse magnetic field with uniform magnetic flux density B_0 effects the flow field. We consider a variable wall temperature distribution of the form $T_w(x) = T_\infty + bx$ in which T_∞ denotes fluid temperature at the ambient and b is a constant. We will apply Oberbeck-Boussinesq approximation to simplify the problem. According to this assumption, the density variations can be ignored everywhere except in the terms appearing with gravitational acceleration. Cross [3] proposed the following relationship between apparent viscosity η and shear rate $\dot{\gamma}$ for shear-thinning fluids:

$$\frac{\eta - \eta_\infty}{\eta_0 - \eta_\infty} = \left(\frac{1}{1 + (K|\dot{\gamma}|)^n} \right). \quad (2.1)$$

In the above equation, η_0 denotes the viscosity at zero shear rate. It is a valuable parameter in assessing the stability of suspensions and emulsions. η_∞ stands for infinite shear rate viscosity which is appropriate in predicting material's response in case of high shearing situations. K is the consistency index or Cross time constant. Here $1/K$ is the critical shear rate which indicates the commencement of deformation. Flow behavior index n is non-dimensional and it measures the dependence of viscosity on deformation rate in the shear-thinning region. Eq. (2.1) gives Newtonian flow behavior when $n \rightarrow 0$, while as $n \rightarrow \infty$, Eq. (1) corresponds to an increasingly shear-thinning response.

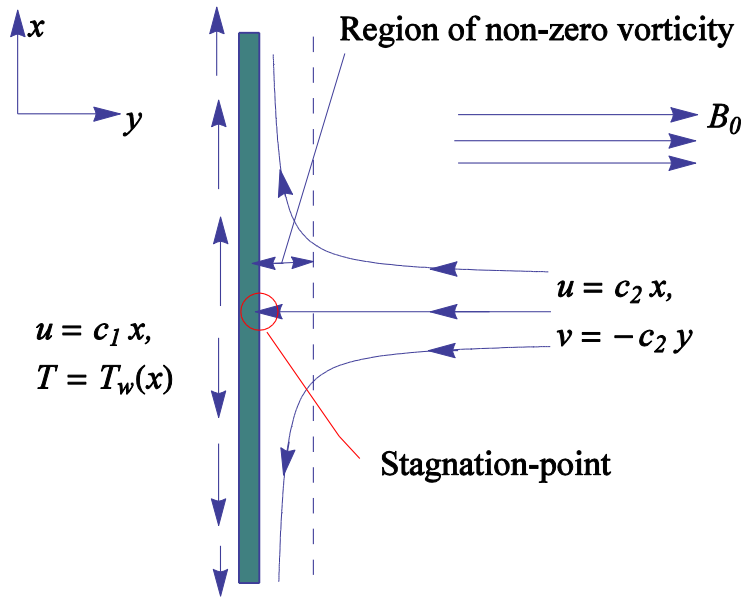


Figure 2.1: Physical sketch of the problem.

Thus extra stress tensor \mathbf{S} for the Cross fluid model is given by [3]

$$\mathbf{S} = 2\eta\mathbf{D} = 2\left(\frac{\eta_0}{1 + (K|\dot{\gamma}|)^n}\right)\mathbf{D}, \quad (2.2)$$

where $\mathbf{D} = \frac{1}{2}[(\nabla\mathbf{V}) + (\nabla\mathbf{V})^t]$ is the deformation rate tensor. The shear rate $\dot{\gamma}$ is given by:

$$\dot{\gamma} = (2D_{kl}D_{kl})^{1/2} = \left(4\left(\frac{\partial u}{\partial x}\right)^2 + \left(\frac{\partial u}{\partial y} + \frac{\partial v}{\partial x}\right)^2\right)^{1/2}. \quad (2.3)$$

In view of Eqs. (2.2) and (2.3), the boundary layer equations embodying the MHD flow around a stagnation with heat transfer are obtained as follows (see Khan et al. [8]):

$$\frac{\partial u}{\partial x} + \frac{\partial v}{\partial y} = 0, \quad (2.4)$$

$$u \frac{\partial u}{\partial x} + v \frac{\partial u}{\partial y} = u_e \frac{du_e}{dx} + v \frac{\partial}{\partial y} \left(\frac{\frac{\partial u}{\partial y}}{1 + \left(K \left| \frac{\partial u}{\partial y} \right| \right)^n} \right) + \frac{\sigma B_0^2}{\rho} (u_e - u) + g\beta_T (T - T_\infty), \quad (2.5)$$

$$\rho c_p \left(u \frac{\partial T}{\partial x} + v \frac{\partial T}{\partial y} \right) = \frac{\partial}{\partial y} \left(k(T) \frac{\partial T}{\partial y} \right). \quad (2.6)$$

Relying on no-slip and no penetration situation at the stretching wall, one has

$$u = u_w(x) = c_1 x, \quad v = 0, \quad T = T_w(x) = T_\infty + bx \text{ at } y = 0, \quad (2.7a)$$

and far field conditions are given below:

$$u \rightarrow u_e(x) = c_2 x, \quad v \rightarrow v_e(y) = -c_2 y, \quad T \rightarrow T_\infty \text{ as } y \rightarrow \infty, \quad (2.7b)$$

where $\nu = \eta_0/\rho$ is the kinematic viscosity of the fluid in which ρ denotes the fluid density, σ indicates the fluid electrical conductivity, B_0 is the magnetic flux density, β_T represents the coefficient of thermal expansion, g denotes the gravitational acceleration, c_p is the specific heat capacity and $k(T) = k_\infty(1 + \epsilon(T - T_\infty)/\Delta T)$ represents variable thermal conductivity in which $\epsilon > 0$ is a constant and k_∞ stands for thermal conductivity of the external flow.

By introducing the following transformations

$$\eta = \sqrt{\frac{c_1}{\nu}} y, \quad \psi = \sqrt{\nu c_1} x f(\eta), \quad \theta(\eta) = \frac{T - T_\infty}{T_w - T_\infty}, \quad (2.8)$$

in which $f(\eta)$ denotes the non-dimensional stream function and $\theta(\eta)$ is the non-dimensional temperature, the continuity equation is already satisfied while momentum equation (2.5) and energy equation (2.6) reduce to the following ordinary differential equations:

$$f''' + \frac{[1 + (We|f''|)^n]^2}{[1 + (1-n)(We|f''|)^n]} [f f'' - f'^2 + M^2(A - f') + A^2 + \lambda \theta] = 0, \quad (2.9)$$

$$(1 + \epsilon \theta) \theta'' + \epsilon \theta'^2 + \text{Pr}(f \theta' - f' \theta) = 0, \quad (2.10)$$

subject to the transformed conditions:

$$\text{at } \eta = 0, \quad f = 0, \quad f' = 1, \quad \theta = 1, \quad (2.11a)$$

$$\text{as } \eta \rightarrow \infty, \quad f' \rightarrow A, \quad \theta \rightarrow 0. \quad (2.11b)$$

In the above equations, $We = c_1 K (Re_x)^{1/2}$ is the local Weissenberg number in which $Re_x = u_w x / \nu$ denotes the local Reynolds number, $M = (\sigma B_0^2 / \rho c_1)^{1/2}$ denotes the magnetic interaction parameter, $Pr = \eta_0 c_p / k$ stands for Prandtl number, $A = c_2 / c_1$ is the stretching rates ratio parameter and $\lambda = g \beta_T b / c_1^2$ denotes the mixed convection parameter (which is also referred as Richardson number).

Positive values of λ indicate that the buoyancy force acts in the same direction as that of the stretching induced flow thereby assisting the fluid motion. Whereas negative values of λ indicate that buoyancy force opposes the fluid flow driven by stretching surface.

Skin friction coefficient C_f , which is of prime importance in many applications, can be obtained from

$$C_f = \frac{\tau_w}{\rho u_w^2 / 2}, \quad (2.12)$$

where τ_w denotes the shear stress at the sheet which is evaluated as follows:

$$\tau_w = \tau_{xy}|_{y=0} = \eta_0 \left(\frac{\frac{\partial u}{\partial y}}{1 + \left(K \left| \frac{\partial u}{\partial y} \right| \right)^n} \right)_{y=0}. \quad (2.13)$$

Using Eq. (2.13), Eq. (2.12) can be expressed as:

$$\frac{1}{2} Re_x^{1/2} C_f = \frac{f''(0)}{1 + (We |f''(0)|)^n}. \quad (2.14)$$

in which $Re_x = u_w x / \nu$ is the local Reynolds number.

Another useful quantity is the local Nusselt number Nu_x defined as follows:

$$Nu_x = \frac{x q_w}{k(T_w(x) - T_\infty)}, \quad (2.15)$$

in which $q_w = -k(\partial T / \partial y)_{y=0}$ is the wall heat flux. Now, application of transformations (2.8) to Eq. (2.15) leads us to the following result:

$$Re_x^{-1/2} Nu_x = -\theta'(0). \quad (2.16)$$

2.2 Numerical results and discussion

Eqs. (2.9) and (2.10) with the conditions (2.11a) and (2.11b) is a two point boundary value problem (BVP) having no exact solution near sight. To numerically solve this third order BVP, we have converted our system into a set of first order initial value problem. Substituting $f = y_1$, $f' = y_2$, $f'' = y_3$, $\theta = y_4$, $\theta' = y_5$, our boundary layer equations are shaped into the following form:

$$\begin{bmatrix} y_1' \\ y_2' \\ y_3' \\ y_4' \\ y_5' \end{bmatrix} = \begin{bmatrix} y_2 \\ y_3 \\ -\frac{[1 + (We|y_3|)^n]^2}{[1 + (1-n)(We|y_3|)^n]} [y_1 y_3 - y_2^2 + M^2(A - y_2) + A^2 + \lambda y_4] \\ y_5 \\ -\frac{1}{(1 + \epsilon y_4)} [\epsilon y_4^2 + Pr(y_1 y_5 - y_2 y_4)] \end{bmatrix}, \quad (2.17)$$

together with the initial conditions:

$$\begin{bmatrix} y_1(0) \\ y_2(0) \\ y_3(0) \\ y_4(0) \\ y_5(0) \end{bmatrix} = \begin{bmatrix} 0 \\ 1 \\ u(1) \\ 1 \\ u(2) \end{bmatrix}, \quad (2.18)$$

where $u(1)$ and $u(2)$ are the approximate initial guesses. This first order initial value problem is solved in MATLAB through shooting technique with RK-5 integration method.

The results are also verified through MATLAB routine `bvp4c` that can tackle non-linear multipoint BVPs. For a detailed implementation of this scheme, the reader is suggested to see the tutorial notes by Shampine et al. [51] or the recent article [52] in which numerical solutions for Bödewadt flow problem are furnished.

Before proceeding with the discussion of our numerical results, it is necessary to verify our code. For this purpose we rely on the published data for Newtonian fluids. Table 2.1 compares the results of $f''(0)$ with those of available article [16] in Newtonian fluid case ($We = 0$). The two data sets appear virtually similar in all the cases which guarantees the accuracy of our code. After verifying the numerical scheme, our interest mainly lies in the brand new graphical results that illustrate the behaviors of consistency index K and flow behavior index n on the similarity solutions.

In figure 2.2, we present similarity solution f' , representing u -velocity component, for different values of mixed convection parameter λ . Fluid velocity near the surface is much enhanced when λ becomes large. From the physical view point, $\lambda > 0$ indicates the heating of surrounding fluid or cooling of stretching surface while negative λ indicates cooling of fluid or heating of stretching surface. For $A < 1$, f' monotonically decreases with increasing η and hence $f''(0)$ has a negative sign. When $A > 1$, f' increases monotonically when η increases and thus $f''(0)$ has a positive sign. Notably a monotonic reduction in boundary layer thickness occurs when parameter A is incremented.

Figure 2.3 shows the u – velocity component, represented by f' , for varying magnetic interaction parameter M . It is clear that boundary layer substantially contracts due to the existence of magnetic force. It is evident that velocity in x –direction increases for increasing values of M when $A > 1$. However for $A < 1$, f' declines as M is increased. It follows from the fact the Lorentz force established due to the transverse magnetic field has a retarding influence on the momentum transport phenomenon.

Figure 2.4 depicts the behavior of the velocity profile upon changing the flow behavior index n . The function f' increases with increasing n when $A < 1$. However opposite trend is witnessed when $A > 1$. A monotonic thickening in boundary layer is observed as the values of n are incremented. This effect is ascribed to the inverse relationship of apparent viscosity with flow behavior index n .

Figure 2.5 demonstrates the variation in u -velocity component f' by varying the local Weissenberg number We . The case $We = 0$ is included for comparison purposes. It is predicted that by varying We , the hydrodynamic boundary layer should become thinner. Physically, when We enlarges the stress relaxation duration becomes large compared with characteristic time scale, leading to the thinning of hydrodynamic boundary layer. This effect leads to higher magnitude of $f''(0)$ or equivalently higher stress at the boundary.

Figure 2.6 displays the evolution of temperature profile $\theta(\eta)$ at different Prandtl numbers. The function θ begins from 1 at the surface and asymptotically vanishes outside the thermal boundary layer. Clearly, an increase in Prandtl number leads to the shrinking of the thermal boundary layer. This is due to the fact that increasing Prandtl number reduces thermal

conductivity and increases thermal resistivity of the fluid thus resulting into reduced heat flow into the fluid. This reduces fluid temperature and produces higher temperature gradient at the boundary.

Figure 2.7 includes the influence of magnetic field on the thermal boundary layer. Upon increasing parameter M fluid attains ambient temperature at a shorter distance above the wall. It means that heat penetration depth is reduced due to the inclusion of transverse magnetic field. Our calculations indicated that horizontal velocity v at far field is also decreased when M is increased. This implies that the amount of cold fluid drawn vertically towards the surface reduces as M becomes large. This in turn leads to the expansion of thermal boundary layer. Figure 2.8 addresses the behavior of variable thermal conductivity parameter ϵ on temperature profile θ . An increasing trend in thermal boundary layer thickness is found when ϵ is varied. This is because fluid thermal diffusivity enhances when ϵ becomes large.

Wall velocity gradient $f''(0)$ (proportional to the skin friction coefficient) is computed as function of local Weissenberg number We in figure 2.9. The flow behavior index n varies between $n = 0.1$ and $n = 0.9$. The magnitude of $f''(0)$ grows with increasing n except when We lies in some small neighborhood of zero. However $f''(0)$ is an increasing function of We at any chosen value of n . In figures 2.10 and 2.11, we present the impact of buoyancy force on $f''(0)$ under both aiding and opposing flow situations. We conclude that resisting force on the surface can be substantially reduced in opposing flow regime.

In Fig. 2.12, the local Nusselt number profiles are obtained against the flow behavior index n at different local Weissenberg numbers. This figure predicts that cooling rate of the surface elevates as parameter n increases. Similar conclusions were drawn in the previous paper by Khan et al. [3]. Figs. 2.13 and 2.14 are prepared to envisage the role of mixed convection parameter λ on local Nusselt number $-\theta'(0)$.

Table 2.2 presents the values of skin friction coefficient $\frac{1}{2}Re_x^{1/2}C_f$ and heat transfer rate $Re_x^{-1/2}Nu_x$ found by changing the values of embedded parameters. It is clear that by increasing power-law index n , the skin friction coefficient should increase with $We = 0.5$. However, a considerable decrease in $\frac{1}{2}Re_x^{1/2}C_f$ is visible when Local Weissenberg number We is varied

from $We = 0$ to $We = 5$. This implies that the force which maintains uniform stretching can be abridged as we increase We . In the existence of assisting/opposing buoyancy force, resisting force at the surface is considerably elevated/ diminished compared with the same without any buoyancy effect. By increasing either magnetic interaction parameter M or the velocity ratio parameter A , we found a growing trend in wall drag coefficient. Similar conclusions was also made in previous papers (see [15], [16], [17] etc.). A marginal rise in local Nusselt number is seen on incrementing the values of flow behavior index n . Also, cooling rate at the surface appears to be a decreasing function of We . Notably, the existence of buoyancy force provides heat transfer enhancement which has vital role in manufacturing related applications.

Table 2.1: Comparison of results for $f''(0)$ with those of [16] in Newtonian fluid case ($We = 0$) when $\lambda = 0$.

M^2	$ f''(0) $			
	$A = 0.2$		$A = 2$	
	Mahapatra et al. [16]	Present	Mahapatra et al. [16]	Present
0	0.9181	0.91811	2.0175	2.01750
0.5	1.0768	1.07682	2.1363	2.13632
1	1.2156	1.21562	2.2491	2.24910
1.5	1.3404	1.34038	2.3567	2.35667
2	1.4546	1.45460	2.4597	2.45967
3	1.6569	1.65979	2.6540	2.65397
5	2.0085	2.00847	3.0058	3.00578
10	2.6892	2.68944	3.7447	3.74471
20	3.6922	3.69223	4.9004	4.90037
40	5.1412	5.14123	6.6339	6.63381
100	8.052	8.05184	10.1934	10.1982
500	17.8617	17.9118	22.4499	22.4499
1000	25.1163	25.3147	31.6858	31.6860

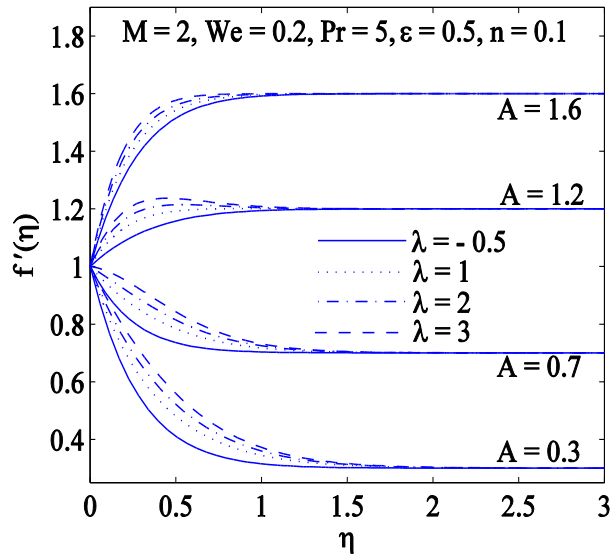


Figure 2.2: Variation in velocity $f'(\eta)$ with η for various values mixed convection parameter λ .

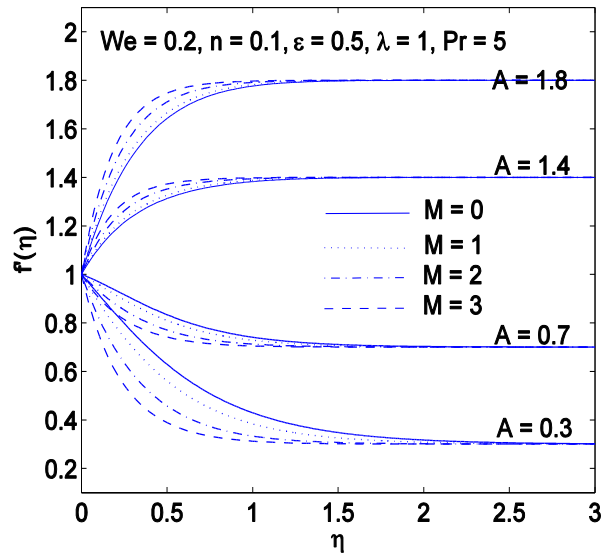


Figure 2.3: Variation in velocity $f'(\eta)$ with η for various values of magnetic interaction parameter M .

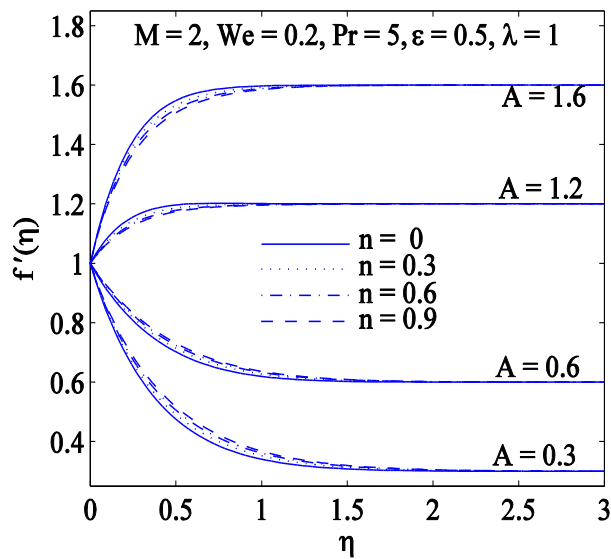


Figure 2.4: Variation in velocity $f'(\eta)$ with η for various values flow behavior index n .

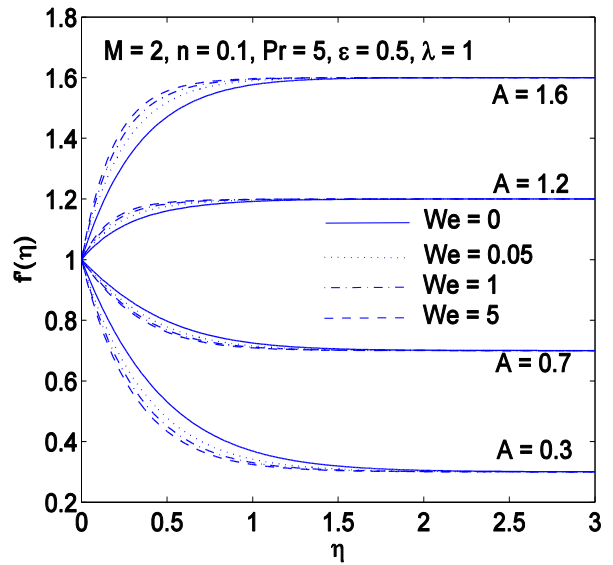


Figure 2.5: Variation in velocity $f'(\eta)$ with η for various values of local Weissenberg number We .

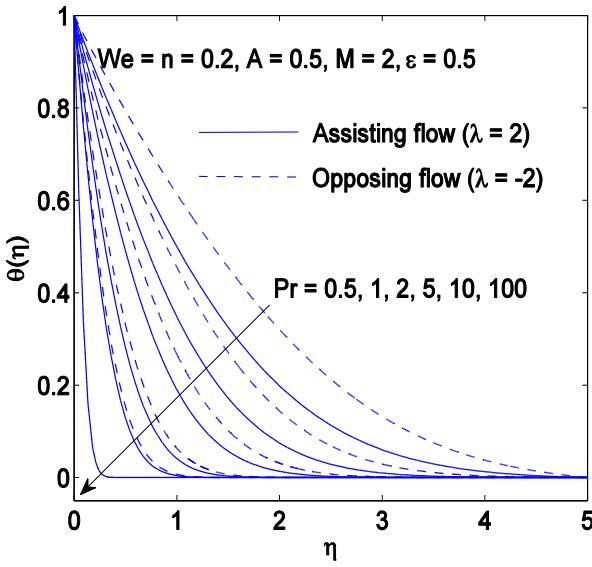


Figure 2.6: Variation in temperature $\theta(\eta)$ with η for various values of Prandtl number Pr .

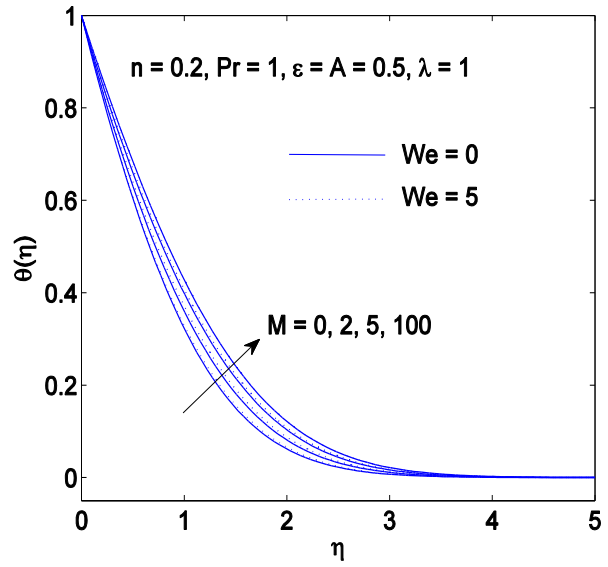


Figure 2.7: Variation in temperature $\theta(\eta)$ with η for various values of magnetic interaction parameter M .

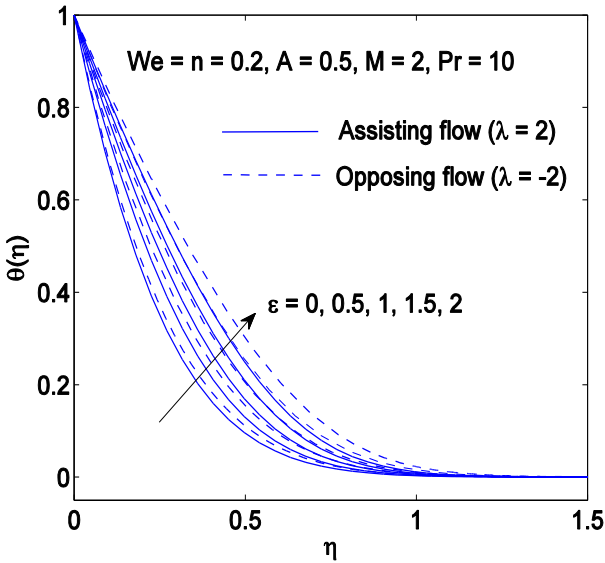


Figure 2.8: Variation in temperature $\theta(\eta)$ with η for various values of parameter ϵ .

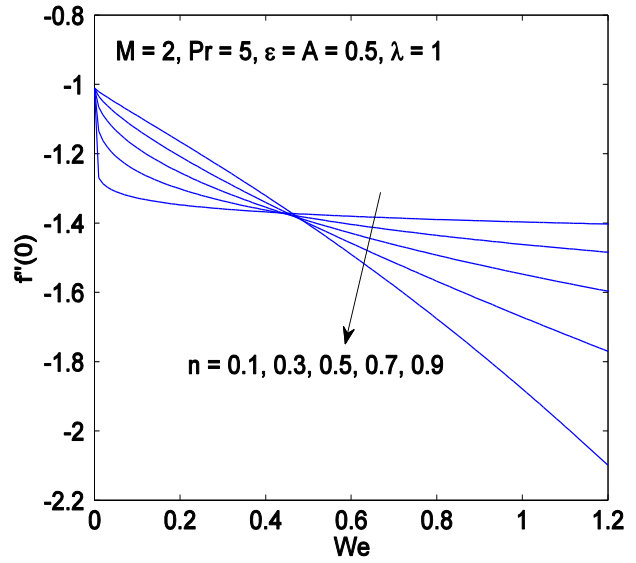


Figure 2.9: Variation in $f''(0)$ with We for various values of flow behavior index n .

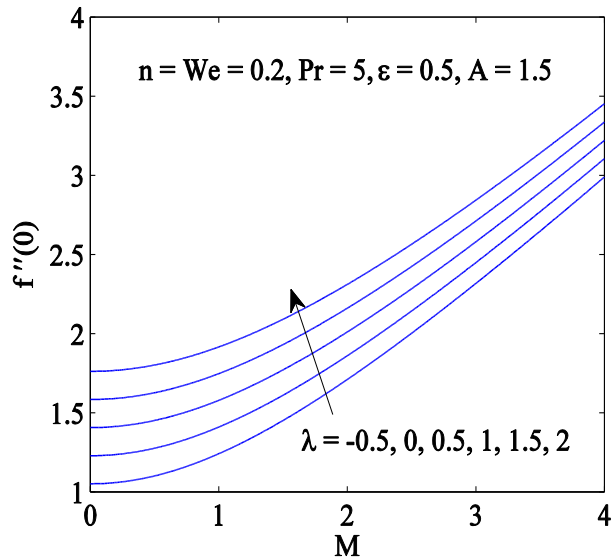


Figure 2.10: Variation in $f''(0)$ with M for various values of mixed convection parameter λ when $A > 1$.

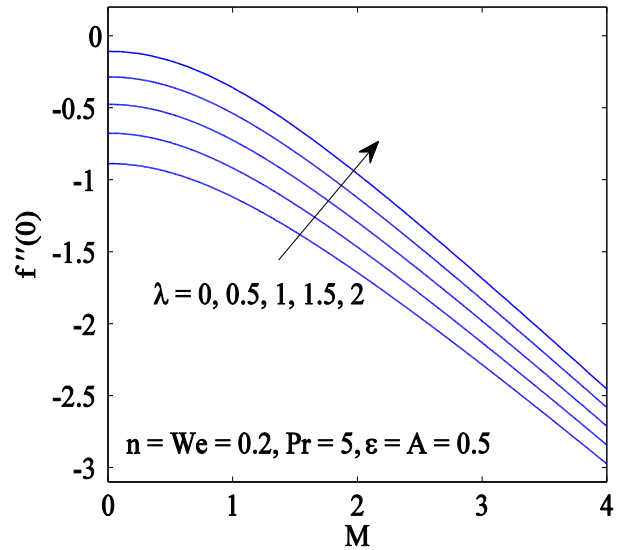


Figure 2.11: Variation in $f''(0)$ with M for various values of mixed convection parameter λ when $A < 1$.

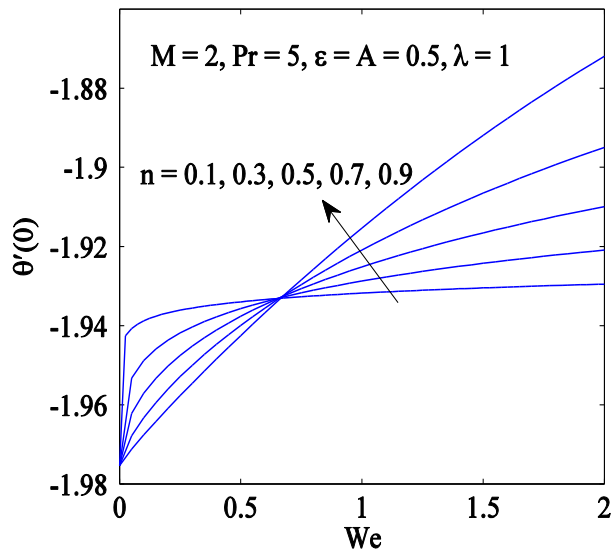


Figure 2.12: Variation in $\theta'(0)$ with We for various values of flow behavior index n .

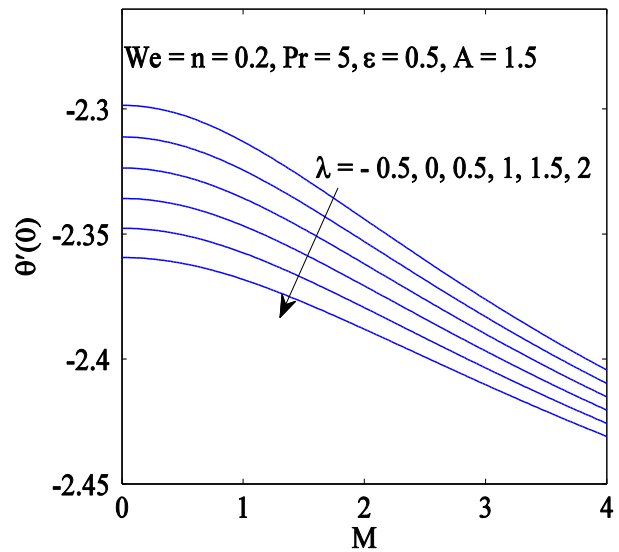


Figure 2.13: Variation in $\theta'(0)$ with M for various values of mixed convection parameter λ when $A > 1$.

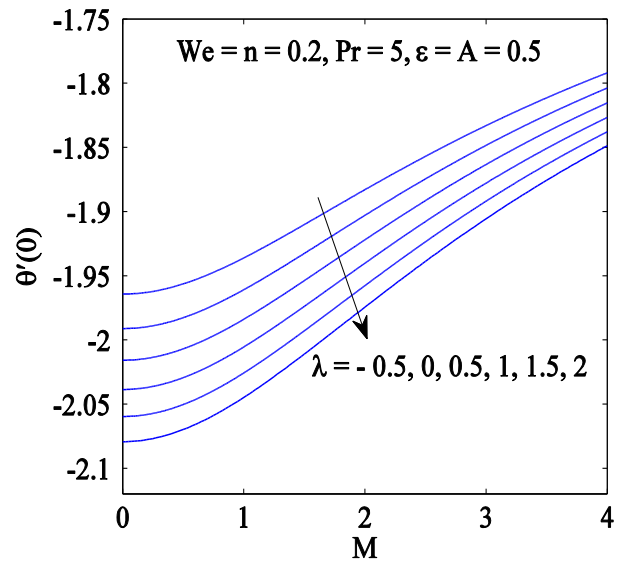


Figure 2.14: Variation in $\theta'(0)$ with M for various values of mixed convection parameter λ when $A < 1$.

Table 2.2: Numerical values of skin friction coefficient and local Nusselt number for various values of We , n , λ , M and ϵ with $Pr = 10$ and $A = 0.5$.

We	n	M	λ	ϵ	$\frac{1}{2}Re_x^{1/2}C_f$		$Re_x^{-1/2}Nu_x$		CPU time (seconds)
					Bvp4c	Shooting method	Bvp4c	Shooting method	
0	0.2	2	1	0.5	-1.03315	-1.03315	2.84802	2.84802	0.57350
0.05					-0.81424	-0.81424	2.81172	2.81172	0.78150
1					-0.70279	-0.70279	2.78861	2.78861	0.73900
5					-0.63422	-0.63422	2.77231	2.77231	0.91625
0.5	0				-0.70062	-0.70062	2.79354	2.79354	0.57225
	0.3				-0.74557	-0.74557	2.79546	2.79546	0.74600
	0.6				-0.78807	-0.78807	2.79810	2.79810	0.78625
	0.9				-0.82684	-0.82684	2.80177	2.80177	0.65350
	0.5	0			-0.36536	-0.36535	2.91490	2.91490	0.80475
		1			-0.49608	-0.49606	2.87689	2.87690	0.76950
		2			-0.77428	-0.77430	2.79711	2.79708	0.75600
		3			-1.08573	-1.08631	2.71414	2.71590	0.67175
		2	0		-0.91428	-0.91428	2.76039	2.76039	0.79325
			0.5		-0.84419	-0.84419	2.77914	2.77914	0.76275
			2		-0.63478	-0.63478	2.83092	2.83092	0.71350
			3		-0.49538	-0.49538	2.86209	2.86209	0.69425
			1	0	-0.78769	-0.78772	3.66788	3.66785	0.73200
				1	-0.76373	-0.76377	2.32754	2.32752	0.74625
				2	-0.74777	-0.74781	1.81433	1.81431	0.78625
				3	-0.73598	-0.73602	1.52921	1.52918	0.79750

2.3 Conclusions

Stagnation-point flow impinging on an isothermal stretching wall immersed in a non-Newtonian Cross fluid is explored. A similarity solution is found which enabled us to depict the behaviors of power-law index (n) and relaxation time constant (K) on the flow and thermal fields. Following observations are noted from the current study:

- The resisting behavior of transverse magnetic field on the momentum transport is visible from the numerical results.

- By increasing the flow behavior index (n), a reduction in wall shear stress occurs for a certain range of Weissenberg number We . This outcome is ascribed to the shear-thinning character of Cross fluid.
- The amount of vertical fluid sucked towards the stretching surface reduces with increasing M . The effect accompanies with a diminution in heat transfer rate.
- Increasing buoyancy force leads to an enhancement in velocity and reduction in and temperature distribution near the surface.
- A considerable decrease in wall drag coefficient is found when local Weissenberg number is increased.
- Heat transfer rate improves/deteriorates when the strength of assisting/opposing buoyancy force is enhanced.

Chapter 3

Pressure driven flow of Cross fluid along a stationary plate subject to binary chemical reaction and Arrhenius activation energy

This chapter discusses the flow of Cross rheological fluid along a stationary rigid plate caused by stream wise pressure gradient. Interaction of flow field with chemically reacting solute is deliberated through the advection-diffusion equation which accounts for temperature dependence of the reaction rate. Energy equation containing source term and fluid with variable thermal conductivity is considered. Locally similar solutions are obtained by the usual transformations. The impact of various parameters on flow, heat and mass transfer of Cross fluid is investigated through numerical computations.

3.1 Problem formulation

Let us consider a flow of shear-thinning fluid obeying Cross rheological model along a flat plate with variable external free stream. The plate resides along the x –axis and fluid occupies the region $y \geq 0$. Let T_w be the constant temperature at the plate and C_w is the solute concentration at the plate. The ambient values of temperature and solute concentration, denoted by T_∞ and C_∞ respectively, are attained at high distance above the plate. Activation energy due to modified Arrhenius function will be considered here. Flow field exhibits for the influence of transverse magnetic field. Invoking customary assumption of small magnetic Reynolds number, the induced magnetic field becomes insignificant in comparison to the applied magnetic field. Cross [3] proposed the following rheological equation of state for shear-thinning fluids:

$$\frac{\eta - \eta_\infty}{\eta_0 - \eta_\infty} = \left(\frac{1}{1 + (K|\dot{\gamma}|)^n} \right), \quad (3.1)$$

where η_0 is the viscosity at zero shear rate, η_∞ is the infinite shear rate viscosity which will be neglected here, K stands for the consistency index, $\dot{\gamma}$ denotes the shear rate and n is the flow behavior index of the fluid.

Accounting (3.1), the extra stress tensor can be expressed as:

$$\mathbf{S} = \eta \mathbf{A}_1 = \left(\frac{\eta_0}{1 + (K|\dot{\gamma}|)^n} \right) \mathbf{A}_1, \quad (3.2)$$

where $\mathbf{A}_1 = (\text{grad}\mathbf{V}) + (\text{grad}\mathbf{V})^t$ denotes the first Rivlin-Ericksen tensor. In view of the aforementioned assumptions, flow, heat and mass transfer are governed by following equations:

$$\frac{\partial u}{\partial x} + \frac{\partial v}{\partial y} = 0, \quad (3.3)$$

$$u \frac{\partial u}{\partial x} + v \frac{\partial u}{\partial y} = u_e \frac{du_e}{dx} + v \frac{\partial}{\partial y} \left(\frac{\frac{\partial u}{\partial y}}{1 + \left(K \left| \frac{\partial u}{\partial y} \right|^n \right)} \right) + \frac{\sigma_1 B_0^2}{\rho} (u_e - u), \quad (3.4)$$

$$\rho c_p \left(u \frac{\partial T}{\partial x} + v \frac{\partial T}{\partial y} \right) = \frac{\partial}{\partial y} \left(k(T) \frac{\partial T}{\partial y} \right) + Q(T - T_\infty), \quad (3.5)$$

$$u \frac{\partial C}{\partial x} + v \frac{\partial C}{\partial y} = D \nabla^2 C - k_r^2 \left(\frac{T}{T_\infty} \right)^m e^{-\frac{E_a}{\kappa T}} (C - C_\infty). \quad (3.6)$$

With no-slip and no-penetration at the plate, one can write:

$$u = 0, \quad v = 0, \quad T = T_w, \quad C = C_w \quad \text{at } y = 0, \quad (3.7a)$$

and at the frictionless regime, we have:

$$u \rightarrow u_e(x) = ax, \quad v \rightarrow v_e(y) = -ay, \quad T \rightarrow T_\infty, \quad C \rightarrow C_\infty \quad \text{as } y \rightarrow \infty, \quad (3.7b)$$

where $\nu = \eta_0/\rho$ represents kinematic viscosity in which ρ stands for the fluid density, σ_1 represents the fluid electrical conductivity, B_0 denotes the constant magnetic flux density, c_p the specific heat capacity, $k(T) = k_\infty(1 + \epsilon(T - T_\infty)/\Delta T)$ the thermal conductivity in which k_∞ denotes thermal conductivity at the ambient and $\epsilon > 0$ is a constant.

The term $Q(T - T_\infty)$ represents the amount of heat transferred per unit volume where Q is a constant. The term $k_r^2(T/T_\infty)^m e^{-E_a/\kappa T}$ represents temperature-dependent reaction rate in which E_a represents the activation energy, $m \in (-1,1)$ denotes the fitted rate constant and $\kappa = 8.61 \times 10^{-5} \text{eV/K}$ is the Boltzmann constant.

Let us introduce the transformations

$$\eta = \left(\frac{u_e}{x\nu}\right)^{\frac{1}{2}} y, \quad u = u_e f'(\eta), \quad v = -\left(\frac{\nu u_e}{x}\right)^{\frac{1}{2}} f(\eta), \quad \theta(\eta) = \frac{T - T_\infty}{T_w - T_\infty}, \quad \phi(\eta) = \frac{C - C_\infty}{C_w - C_\infty}, \quad (3.8)$$

where $f(\eta)$ is the non-dimensional stream function, $\theta(\eta)$ the non-dimensional temperature and $\phi(\eta)$ represents the non-dimensional concentration, the continuity equation (3.3) is fulfilled while Eqs. (3.4)- (3.6) convert into the following ODEs:

$$f'''' + \frac{[1 + (We|f''|)^n]^2}{[1 + (1-n)(We|f''|)^n]} [ff'' - f'^2 + M^2(1 - f') + 1] = 0, \quad (3.9)$$

$$(1 + \epsilon\theta)\theta'' + \epsilon\theta'^2 + Pr(f\theta' + s\theta) = 0, \quad (3.10)$$

$$\phi'' + Scf\phi' - Sc\sigma(1 + \delta\theta)^m e^{-\left(\frac{E}{1+\delta\theta}\right)} \phi = 0 \quad (3.11)$$

The boundary conditions (3.7a) and (3.7b) are transformed as

$$f(0) = 0, \quad f'(0) = 0, \quad \theta(0) = 1, \quad \phi(0) = 1, \quad (3.12a)$$

$$f'(+\infty) = 1, \quad \theta(+\infty) = 0, \quad \phi(+\infty) = 0. \quad (3.12b)$$

In Eqs. (3.9)-(3.11), $We = aK(Re_x)^{1/2}$ denotes the local Weissenberg number in which $Re_x = u_e x/\nu$ denotes the local Reynolds number, $M = (\sigma_1 B_0^2/\rho a)^{1/2}$ represents the magnetic interaction parameter, $Pr = \eta_0 c_p/k$ stands for Prandtl number, $s = Q/a\rho c_p$ for the heat source/sink parameter, $Sc = \nu/D$ for Schmidt number, $\sigma = k_r^2/a$ is the dimensionless reaction parameter, $\delta = \Delta T/T_\infty$ is the temperature difference parameter and $E = E_a/(\kappa T_\infty)$ denotes the dimensionless activation energy.

We are primarily interested in evaluating local Skin friction coefficient C_f at the plate defined by:

$$C_f = \frac{\tau_w}{\rho u_e^2/2}, \quad (3.13)$$

where τ_w denotes shear stress at the plate which is obtained as follows:

$$\tau_w = \tau_{xy}|_{y=0} = \eta_0 \left(\frac{\frac{\partial u}{\partial y}}{1 + \left(K \left|\frac{\partial u}{\partial y}\right|\right)^n} \right)_{y=0} = \eta_0 \left(\frac{a(Re_x)^{\frac{1}{2}}}{1 + (We f''(0))^n} \right). \quad (3.14)$$

Using Eq. (3.14) and the transformations (3.8), Eq. (3.14) takes the following form:

$$\frac{1}{2}Re_x^{\frac{1}{2}}C_f = \frac{f''(0)}{1 + (We|f''(0)|)^n}, \quad (3.15)$$

in which $Re_x = u_e x / \nu$ is the local Reynolds number.

In order to compute heat and mass transfer rates from the solid surface, we define local Nusselt number Nu_x and local Sherwood number Sh_x :

$$Nu_x = \frac{xq_w}{k(T_w - T_\infty)}, Sh_x = \frac{xj_w}{D(C_w - C_\infty)} \quad (3.16)$$

where $q_w = -k(\partial T / \partial y)_{y=0}$ is the wall heat flux and $j_w = -D(\partial C / \partial y)_{y=0}$ denotes wall mass flux. Inserting these expressions in Eq. (3.16) and then using transformations (3.8), it is easy to verify that:

$$Re_x^{-\frac{1}{2}}Nu_x = -\theta'(0), Re_x^{-\frac{1}{2}}Sh_x = -\phi'(0). \quad (3.17)$$

3.2 Method of solution

The differential system posed by Eqs. (3.9)-(3.11) subject to the conditions (3.12a) and (3.12b) has been solved numerically by employing MATLAB package `bvp4c` that is known for producing accurate numerical results for multipoint boundary value problems. To begin, we reduce the system (3.9)-(3.11) into a first order system by substituting $y_1 = f, y_2 = f', y_3 = f'', y_4 = \theta, y_5 = \theta', y_6 = \phi$ and $y_7 = \phi'$. We obtain the following:

$$y_1' = y_2, \quad (3.18)$$

$$y_2' = y_3, \quad (3.19)$$

$$y_3' = -\frac{\{1 + (We|y_3|)^n\}^2}{\{1 + (1-n)(We|y_3|)^n\}} \{y_1 y_3 - y_2^2 + M^2(1 - y_2) + 1\}, \quad (3.20)$$

$$y_4' = y_5, \quad (3.21)$$

$$y_5' = -\frac{1}{(1 + \epsilon y_4)} \{\epsilon y_4^2 + Pr(y_1 y_5 - s y_4)\}, \quad (3.22)$$

$$y_6' = y_7, \quad (3.23)$$

$$y_7' = -Sc \left\{ y_1 y_7 - \sigma(1 + \delta y_4)^m \exp\left(\frac{-E}{1 + \delta y_4}\right) y_6 \right\}. \quad (3.24)$$

The above set of equations with the respective conditions are directly substituted in solver `bvp4c`. The residual of the boundary conditions is chosen to be uniformly small. For detailed implementation of the solver `bvp4c`, the reader is referred to Ref. [51].

3.3 Results and discussion

Here our interest is to perceive the importance of embedded parameters on the solutions by displaying graphical illustrations. Fig. 3.1 demonstrates the variation in u -velocity component with vertical distance η for various values of Weissenberg number We . The function f' is zero at the plate and tends to unity as $\eta \rightarrow \infty$. It is clear that by increasing Weissenberg number, the boundary layer thickness reduces sharply. This reduction is accompanied by a higher wall velocity gradient $f''(0)$. Fig. 3.2 indicates that boundary layer effects extend up to higher vertical distance when higher flow behavior index n is chosen. Such outcome suggests that skin friction coefficient can be lowered by increasing n . Such behavior is reminiscent of shear-thinning characteristic of Cross fluid. In Fig. 3.3, we plot u -velocity component f' for a variety of magnetic interaction parameters. Similar to the findings of chapter 2, boundary layer shrinks upon increasing magnetic field strength. Thus we anticipate wall shear to enhance as parameter M becomes large. Consequently, the function f' appears to be an increasing function of M . Physically Lorentz force established as a result of transverse magnetic field resists the momentum transport due to which boundary layer suppresses.

Our computations detect that v -velocity component, represented by f , also enhances with increasing parameter M . This in turn increases the amount of cold fluid drawn towards the plate due to which thermal boundary layer suppresses. In Fig. 3.5, temperature curves are computed for wide range of heat source/sink parameter s . An expansion in thermal boundary layer becomes apparent as parameter ($s > 0$) becomes large. However opposite trend is detected by increasing heat sink parameter ($s < 0$). Therefore we conclude that heat transfer from the plate improves/deteriorates as heat sink/source effect intensifies. Fig. 3.6 portrays the change in temperature profile with η at a variety of Prandtl numbers. By increasing Prandtl number, momentum diffusion effect becomes strong in comparison to the thermal diffusion which leads to the thinning of thermal penetration depth and improvement in heat transfer rate from solid

boundary. Fig. 3.7 displays the variation in temperature profile $\theta(\eta)$ by changing the parameter ϵ . Thermal conductivity expression suggests that thermal conductivity varies linearly within the boundary layer with change in temperature. Thus higher value of ϵ leads to a pronounced heat conduction and reduced magnitude of local Nusselt number.

Fig. 3.8 demonstrates the effect of reaction rate parameter σ on concentration profile $\phi(\eta)$. The general trend of concentration ϕ is analogous to that of temperature θ in nearly all the cases. As anticipated, solute concentration is diminished within the boundary layer as generative reaction rate is increased. Fig. 3.9 shows the evolution of concentration profile at a variety of Schmidt numbers. Concentration boundary layer shrinks as Schmidt number Sc becomes large. Physically, an increase in Sc implies a reduction in mass diffusivity which results in enhanced mass transfer of solute from the plate resulting into higher concentration gradient at the plate surface. To envisage the role of fitted rate constant m in the development of concentration boundary layer, Fig. 3.10 is prepared. It appears that behavior of m on ϕ is qualitatively similar to that of σ . Activation energy refers to the least amount of energy required to initiate chemical reaction. Modified Arrhenius function $k_r^2(T/T_\infty)^m e^{\frac{-E_a}{kT}}$, representing reaction rate, is expected to decrease/increase with increasing Activation energy/fluid temperature. Thus increasing parameter E favors destructive chemical reaction rate. This in turn elevates the solute concentration ϕ . In Fig. 3.12, the variation in ϕ with increasing parameter δ is portrayed. By increasing this parameter, wall and ambient temperature difference enlarges which leads to a pronounced heat transfer. Importance of Arrhenius function, therefore increases with increasing δ which in turn leads to a reduction in concentration boundary layer thickness.

Figs. 3.13 and 3.14 show the influences of Weissenberg number We and activation energy on local Sherwood number. The absolute value of $\phi'(0)$ approaches a constant value as activation energy for chemical reaction becomes large. The parameter σ is seen to enhance the mass transfer rate from the plate. Note that the fitted rate constant m also boosts the mass transfer rate.

Table 3.1 includes the local Nusselt number data obtained by varying the rheological parameters of Cross fluid model. The rate of heat transfer is slightly lowered as the flow behavior index n enlarges. A modest elevation in the absolute wall temperature gradient is depicted as Weissenberg number (We) is incremented.

In table 3.2, we enlist the data of local Sherwood number found by varying embedded parameters. Increasing trend in local Sherwood number is observed when either chemical reaction rate or wall and ambient temperature difference enlarges. Similar behavior is noticed when Schmidt number becomes large. However, opposite trend is observed on increasing the value of activation energy.

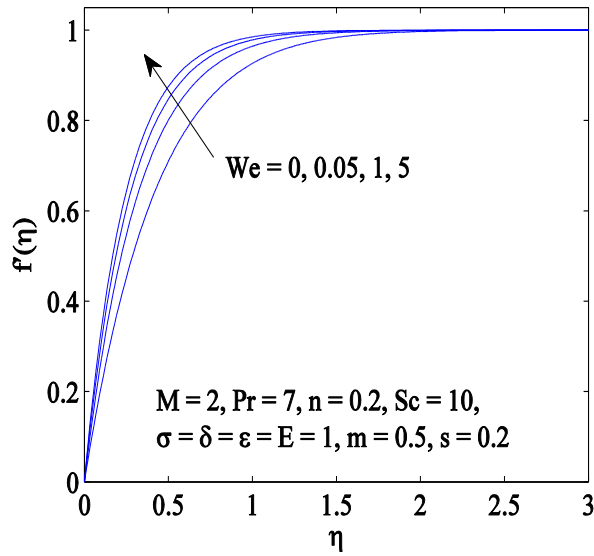


Fig. 3.1: Variation in velocity $f'(\eta)$ with η for various values of local Weissenberg number We .

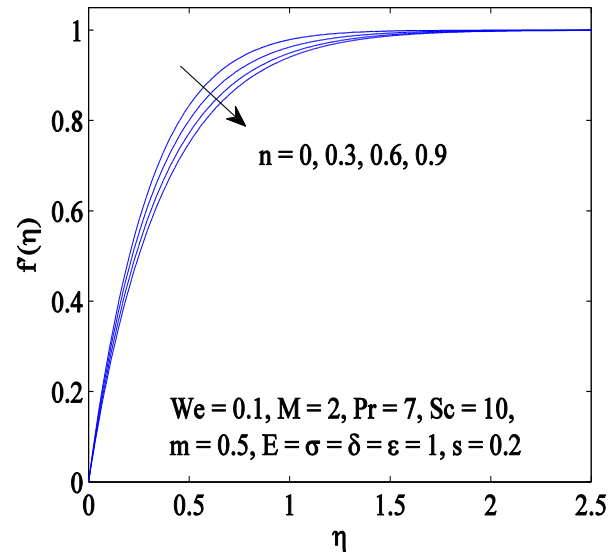


Fig. 3.2: Variation in velocity $f'(\eta)$ with η for various values of flow behavior index n .

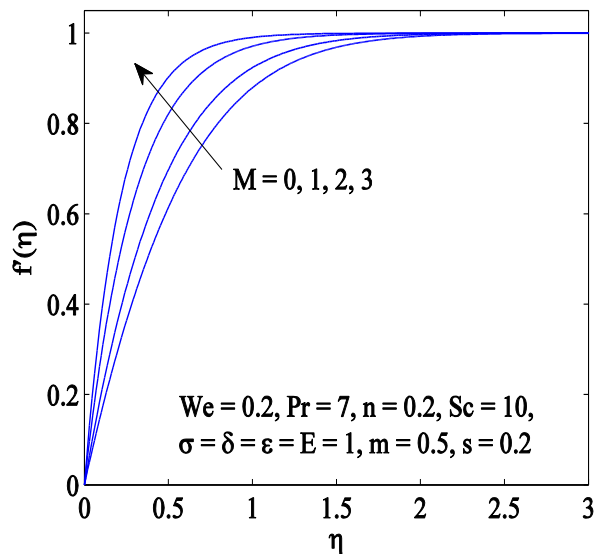


Fig. 3.3: Variation in velocity $f'(\eta)$ with η for various values of magnetic interaction parameter M .

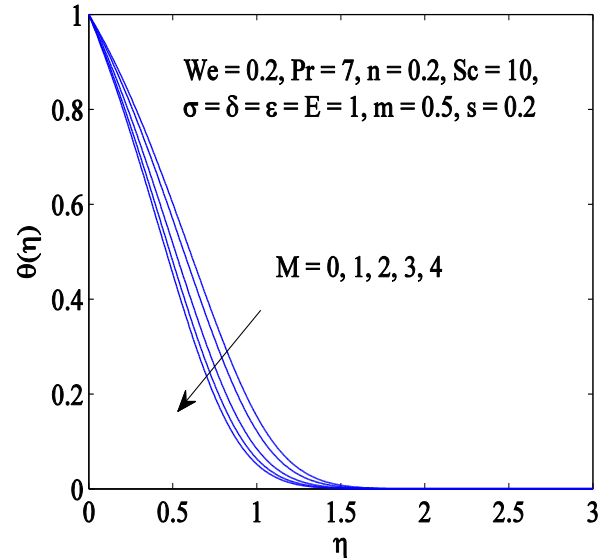


Fig. 3.4: Variation in temperature $\theta(\eta)$ with η for various values of magnetic interaction parameter M .

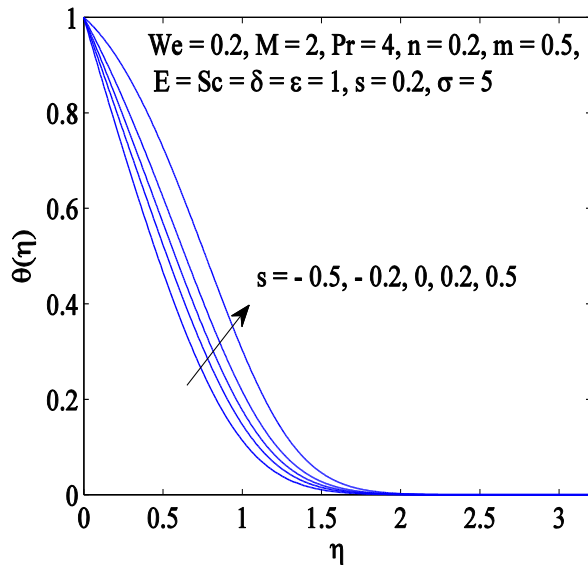


Fig. 3.5: Variation in temperature $\theta(\eta)$ with η for various values of heat source/sink parameter s .

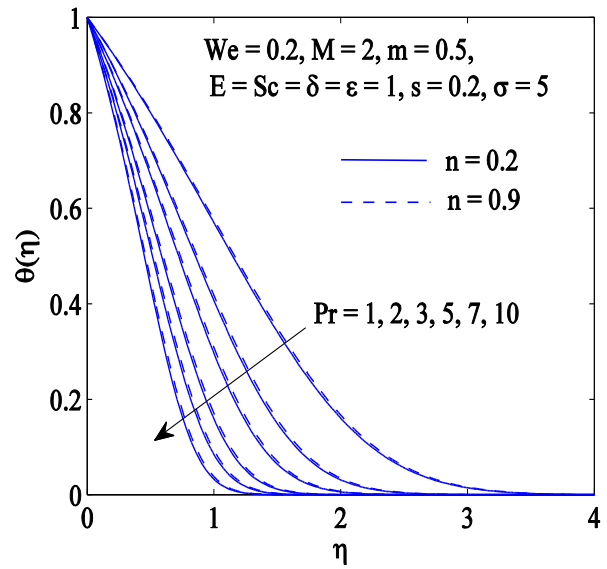


Fig. 3.6: Variation in temperature $\theta(\eta)$ with η for various values of Prandtl number Pr .

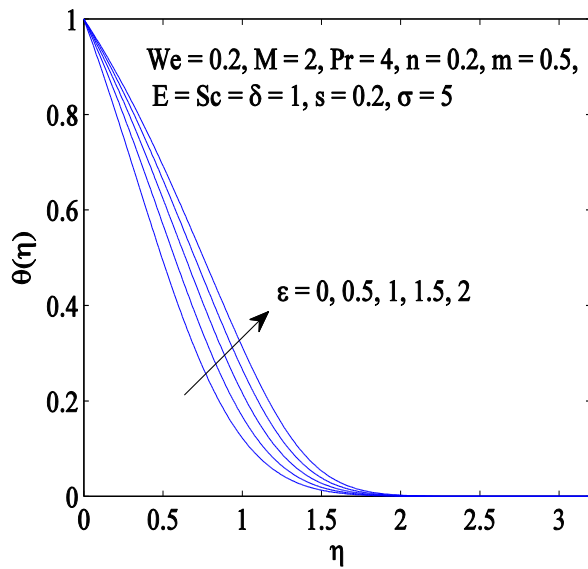


Fig. 3.7: Variation in temperature $\theta(\eta)$ with η for various values of parameter ε .

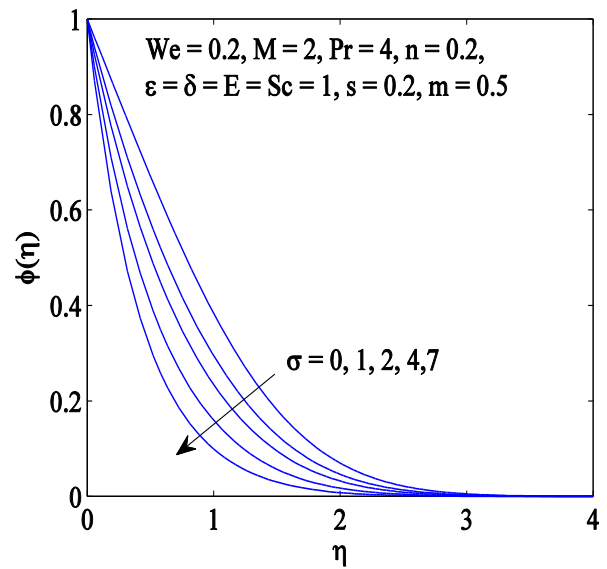


Fig. 3.8: Variation in concentration $\phi(\eta)$ with η for various values of parameter σ .

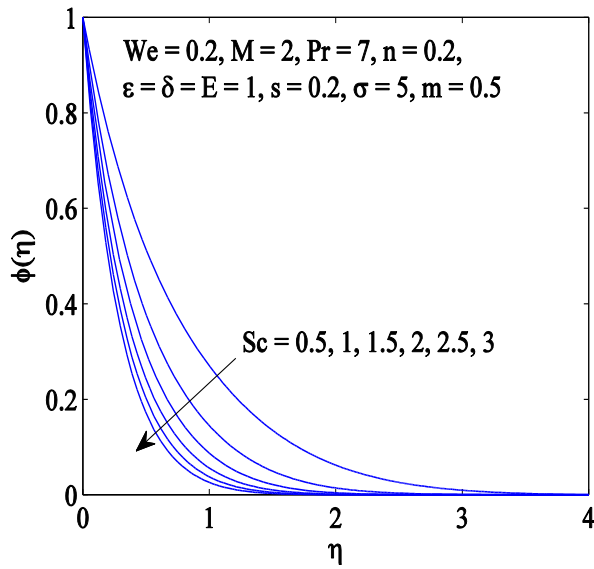


Fig. 3.9: Variation in concentration $\phi(\eta)$ with η for various values of Schmidt number Sc .

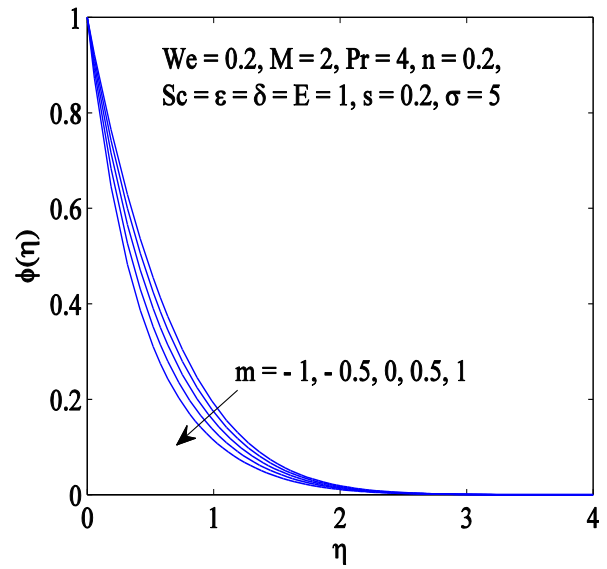


Fig. 3.10: Variation in concentration $\phi(\eta)$ with η for various values of fitted rate constant m .

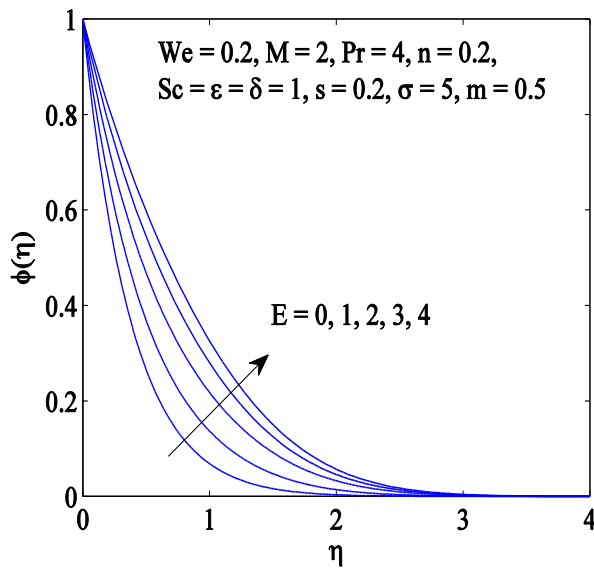


Fig. 3.11: Variation in concentration $\phi(\eta)$ with η for various values of activation energy E .

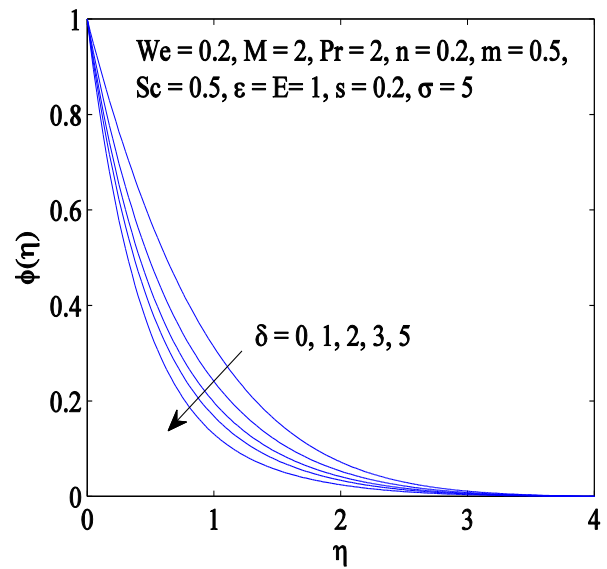


Fig. 3.12: Variation in concentration $\phi(\eta)$ with η for various values of δ .

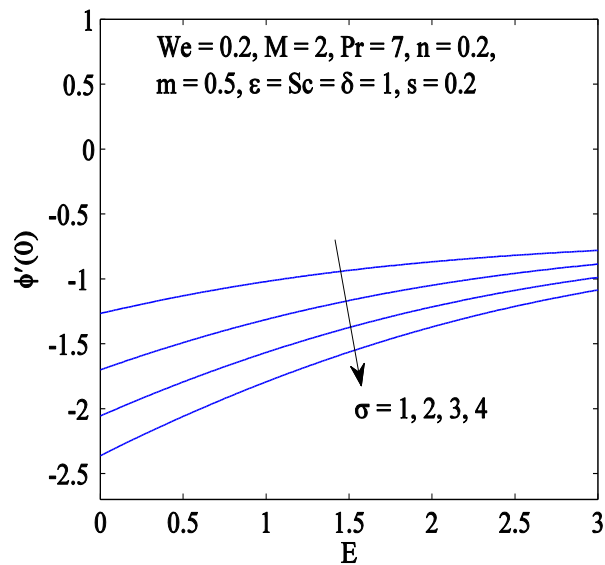


Fig. 3.13: Variation in $\phi'(0)$ with E for various values of σ .

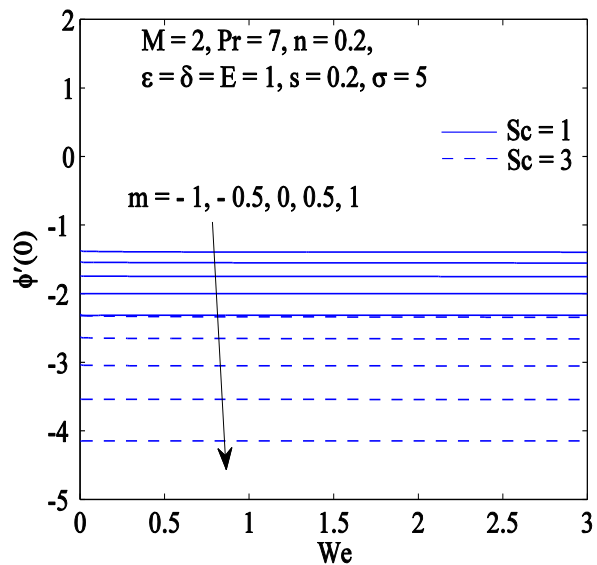


Fig. 3.14: Variation in $\phi'(0)$ with We for various values of m .

Table 3.1: Computational results of local Nusselt number for varying values of We and n with $\sigma = \delta = E = Sc = \epsilon = 1$, $m = 0.5$, $s = 0.2$ and $Pr = 5$.

We	n	$Re_x^{-\frac{1}{2}} Nu_x$
0.1	0.2	0.65752
0.3		0.66842
0.5		0.67388
0.7		0.67761
0.2	0.1	0.66674
	0.3	0.66174
	0.5	0.65647
	0.7	0.65093

Table 3.2: Computational results of local Sherwood number for varying values of σ , δ , E , Sc , m when $We = 0.2$, $n = 0.2$, $M = 2$, $s = 0.2$ and $\epsilon = 1$.

σ	δ	E	Sc	m	$Re_x^{-\frac{1}{2}}Sh_x$
0	1	1	1	0.5	0.66637
1					1.02822
2					1.32638
3					1.58330
1	0				0.86964
	2				1.15121
	3				1.25080
	4				1.33470
	1	0			1.27215
		2			0.87439
		3			0.78405
		4			0.73273
		5			0.70389
		1	2		1.44872
			3		1.76654
			4		2.03170
			5		2.26353
			1	-1	0.85029
				-0.5	0.89489
				0	0.95286
				1	1.12611
				0.5	1.02425

3.4 Concluding remarks

Boundary layer flow of Cross rheological fluid along a static plate with stream wise pressure gradient is analyzed. The flow field is influenced by diffusion of chemically reactive species from the plate. Modified Arrhenius is introduced to account for temperature dependence of reaction rate. Accurate numerical results are achieved for full range of embedded parameters. Main outcomes of this analysis are listed below:

- At a point inside the boundary layer, heat source parameter ($s > 0$) enhances fluid temperature whereas heat sink parameter ($s < 0$) does the reverse.

- Boundary layer effects extend up to a higher axial distance when larger value of n is accounted.
- It is natural to see an expansion in thermal boundary layer as parameter ϵ becomes large.
- Concentration boundary layer expands as activation energy E_a enlarges.
- A slight rise in thermal/solutal penetration depth occurs for increasing shear thinning effect.
- Increasing strength of generative chemical reaction leads to the thinning of concentration boundary layer.

References

1. M. M. Cross, Rheology of non-Newtonian fluids: A new flow equation for pseudoplastic systems, *J. Colloid Sci.* 20 (1965) 417-437.
2. R. B. Bird, C. F. Curtiss, R. C. Armstrong and O. Hassager, *Dynamics of Polymeric Liquids*, Wiley, Newyork, 1987.
3. M. S. Miah, M. S. Hossain, M. A. Ashraf, S. Al-Assaf and A. McMillan, Numerical simulation of non-Newtonian polymer film flow on a rotating spoked annulus, *J. Appl. Pol. Sci.* 134 (2017) <https://doi.org/10.1002/app.44943>.
4. J. Xie and Y. C. Jin, Parameter determination for the Cross rheology equation and its application to modeling non-Newtonian flows using the WC-MPS method, *Eng. Appl. Comp. Fluid Mech.* 10 (2016) 111-129.
5. M. I. Khan, M. Waqas, T. Hayat and A. Alsaedi, Magneto-hydrodynamical numerical simulation of heat transfer in MHD stagnation point flow of Cross fluid model towards a stretched surface, *Phys. Chem. Liq.* (2017), doi: 10.1080/00319104.2017.1367791
6. M. Khan, M. Manzoor and M. Rahman, Boundary layer flow and heat transfer of Cross fluid over a stretching sheet, *Therm. Sci.* (In Press) (2017).
7. M. Khan, M. Manzoor and M. Rahman, On axisymmetric flow and heat transfer of Cross fluid over a radially stretching sheet, *Res. Phys.* 7 (2017) 3767-3772.
8. M. I. Khan, T. Hayat, M. I. Khan and A. Alsaedi, Activation energy impact in nonlinear radiative stagnation point flow of Cross nanofluid, *Int. Commun. Heat & Mass Transf.* 91 (2018) 216-224.
9. K. Hiemenz, Die Grenzschicht an einem in den gleichförmigen Flüssigkeitsstrom eingetauchtengeraden Kreiszyylinder, *Dinglers Polytech. J.* 326 (1911) 321 - 324.
10. F. Homann, Der Einfluss grosser Zähigkeit bei der Stromung um den Zylinder und um den Kugel, *Z. für Angew. Math. und Mech.* 16 (1936) 153-164.
11. T. C. Chiam, Stagnation-point flow towards a stretching plate, *J. Phys. Soc. Jpn.* 63 (1994) 2443-2444.
12. T. R. Mahapatra and A. S. Gupta, Heat transfer in stagnation-point flow towards a stretching sheet, *Heat Mass Transfer* 38 (2002) 517-521.

13. A. Ishak, R. Nazar, N. Amin, D. Filip and I. Pop, Mixed convection in the stagnation-point flow towards a stretching vertical permeable sheet, *Malaysian. J. Math. Sci.* 2 (2007) 217-226.
14. C. Y. Wang, Stagnation flows with slip: Exact solutions of the Navier-Stokes equations, *Z. fürAngew. Math. Phys. (ZAMP)* 54(2003)184-189
15. T. R. Mahapatra and A. S. Gupta, Stagnation-point flow of a viscoelastic fluid towards a stretching surface, *Int. J. Non-linear Mech.* 39 (2004) 811-820.
16. T. R. Mahapatra, S. K. Nandy and A. S. Gupta, Magnetohydrodynamic stagnation-point flow of a power-law fluid towards a stretching surface, *Int. J. Non-linear. Mech.* 44 (2009) 124-129.
17. T. R. Mahapatra, S. K. Nandy and A. S. Gupta, Analytical solution of magnetohydrodynamic stagnation-point flow of a power-law fluid towards a stretching surface, *Appl. Math. Comput.* 215 (2009) 1696-1710.
18. R. Nazar, N. Amin, D. Filip and I. Pop, Stagnation-point flow of a micropolar fluid towards a stretching sheet, *Int. J. Nonlinear Mech.* 39 (2004) 1227-1235.
19. N. Bachok, A. Ishak and I. Pop, Melting heat transfer in boundary layer stagnation-point flow towards a stretching/shrinking sheet, *Phys. Lett. A*, 374 (2010) 4075-4079.
20. A. Mushtaq, M. Mustafa, T. Hayat and A. Alsaedi, Effect of thermal radiation on the stagnation-point flow of upper-convected Maxwell fluid over a stretching sheet, *J. Aerosp. Engg.* 27 (2014) [https://doi.org/10.1061/\(ASCE\)AS.1943-5525.0000361](https://doi.org/10.1061/(ASCE)AS.1943-5525.0000361).
21. M. Mustafa, A. Mushtaq, T. Hayat and A. Alsaedi, Model to study the non-linear radiation heat transfer in the stagnation-point flow of power-law fluid, *Int. J. Numer. Meth. Heat & Fluid Flow* 25 (2015) 1107-1119.
22. M. Shen, F. Wang and H. Chen, MHD mixed convection slip flow near a stagnation-point on a nonlinearly vertical stretching sheet, *Bound. Val. Prob.* 78 (2015) <https://doi.org/10.1186/s13661-015-0340-6>.
23. M. Mustafa, A. Mushtaq, T. Hayat and A. Alsaedi, Non-aligned MHD stagnation-point flow of upper-convected Maxwell fluid with nonlinear thermal radiation, *Neural Comput. Applicat.* (2016) <https://doi.org/10.1007/s00521-016-2761-2>.

24. K. Naganthran, R. Nazar and I. Pop, Unsteady stagnation-point flow and heat transfer of a special third grade fluid past a permeable stretching/shrinking sheet, *Scientific Reports* 6 (2016) doi: 10.1038/srep24632.
25. S. Mansur, A. Ishak and I. Pop, The magnetohydrodynamic stagnation point flow of a nanofluid over a stretching/shrinking sheet with suction, *PLoS ONE* 10 (2016) e0117733. <https://doi.org/10.1371/journal.pone.0117733>.
26. M. M. Rashidi, S. Abelman and N. F. Mehr, Entropy generation in steady MHD flow due to a rotating porous disk in a nanofluid, *Int. J. Heat & Mass Transf.* 62 (2013) 515-525.
27. M. M. Rashidi, M. Ali, N. F. Mehr and F. Nazari, Parametric analysis and optimization of entropy generation in unsteady MHD flow over a stretching rotating disk using artificial neural network and particle swarm optimization algorithm, *Energy* 55 (2013) 497-510.
28. M. M. Rashidi, N. Kavyani and S. Abelman, Investigation of entropy generation in MHD and slip flow over a rotating porous disk with variable properties, *Int. J. Heat & Mass Transf.* 70 (2014) 892-917.
29. M. Sheikholeslami, K. Vajravelu and M. M. Rashidi, Forced convection heat transfer in a semi annulus under the influence of a variable magnetic field, *Int. J. Heat & Mass Transf.*, 92 (2016) 339-348.
30. M. M. Bhatti, M. M. Abbas and M. M. Rashidi, A robust numerical method for solving stagnation point flow over a permeable shrinking sheet under the influence of MHD, *Appl. Math. Comput.* 316 (2018) 381-389.
31. P. R. Sharma, S. Sinha, R. S. Yadav and A. N. Flippov, MHD mixed convective stagnation point flow along a vertical stretching sheet with heat source/sink, *Int. J. Heat & Mass Transf.* 117 (2018) 780-786.
32. A. A. Afify and N. S. Elgazery, Effect of a chemical reaction on magnetohydrodynamic boundary layer flow of a Maxwell fluid over a stretching sheet with nanoparticles, *Particuology* 29 (2016) 154-161.
33. Y. H. Zhuang, H. Z. Yu and Q. Y. Zhu, A thermal non-equilibrium model for 3D double diffusive convection of power-law fluids with chemical reaction in the porous medium, *Int. J. Heat & Mass Transf.* 115 (2017) 670-694.

34. R. Malik and M. Khan, Numerical study of homogeneous–heterogeneous reactions in Sisko fluid flow past a stretching cylinder, *Res. Phys.* 8 (2018) 64-70.
35. T. Hayat, M. W. A. Khan, M. I. Khan, M. Waqas and A. Alsaedi, Impact of chemical reaction in fully developed radiated mixed convective flow between two rotating disk, *Physica B: Cond. Matter* 538 (2018) 138-149.
36. S. O. Adesanya, H. A. Ogunseye and S. Jangili, Unsteady squeezing flow of a radiative Eyring-Powell fluid channel flow with chemical reactions, *Int. J. Thermal Sci.* 125 (2018) 440-447.
37. T. Hayat, M. Waqas, M. Ijaz Khan and A. Alsaedi, Impacts of constructive and destructive chemical reactions in magnetohydrodynamic (MHD) flow of Jeffrey liquid due to nonlinear radially stretched surface, *J. Mol. Liq.* 225 (2017) 302-310.
38. J. Lu, S. Das, E. A. J. F. Peters and J. A. M. Kuipers, Direct numerical simulation of fluid flow and mass transfer in dense fluid-particle systems with surface reactions, *Chem. Eng. Sci.* 176 (2018) 1-18.
39. Hashim, M. Khan, A. S. Alshomrani and R. Haq, Investigation of dual solutions in flow of a non-Newtonian fluid with homogeneous–heterogeneous reactions: Critical points, *Eur. J. Mech. B/Fluids* 68 (2018) 30-38.
40. M. Turkyilmazoglu, Analytical solutions to mixed convection MHD fluid flow induced by a nonlinearly deforming permeable surface, *Commun. Nonlinear Sci. Numer. Simul.* In press (2018); <https://doi.org/10.1016/j.cnsns.2018.04.002>.
41. J. A. Khan and M. Mustafa, A numerical analysis for non-linear radiation in MHD flow around a cylindrical surface with chemically reactive species, *Res. Phys.* 8 (2018) 963-970.
42. A. R. Bestman, Natural convection boundary layer with suction and mass transfer in a porous medium, *Int. J. Energy Res.* 14 (1990) 389-396.
43. O. D. Makinde, P. O. Olanrewaju and W. M. Charles, Unsteady convection with chemical reaction and radiative heat transfer past a flat porous plate moving through a binary mixture, *Afrika Matematika* 22 (2011) 65-78.
44. K. A. Maleque, Effects of binary chemical reaction and activation energy on MHD boundary layer heat and mass transfer flow with viscous dissipation and heat generation/absorption, *ISRN Thermodyn.* 2013 (2013), Article ID 284637; doi: [10.1155/2013/284637](https://doi.org/10.1155/2013/284637).

45. K. A. Maleque, Effects of exothermic/endothemic chemical reactions with Arrhenius activation energy on MHD free convection and mass transfer flow in presence of thermal radiation, *J. Thermodyn.* 2013 (2013), Article ID 629516; doi: [10.1155/2013/692516](https://doi.org/10.1155/2013/692516).
46. F. G. Awad, S. Motsa and M. Khumalo, Heat and mass transfer in unsteady rotating fluid flow with binary chemical reaction and activation energy, *PLOS ONE* 9 (2014) e107622; doi: [10.1371/journal.pone.0107622](https://doi.org/10.1371/journal.pone.0107622).
47. Z. Shafique, M. Mustafa and A. Mushtaq, Boundary layer flow of Maxwell fluid in rotating frame with binary chemical reaction and activation energy, *Res. Phys.* 6 (2016) 627–633.
48. Z. Abbas, M. Sheikh and S. S. Motsa, Numerical solution of binary chemical reaction on stagnation-point flow of Casson fluid over a stretching/shrinking sheet with thermal radiation, *Energy* 95 (2016) 12-20.
49. M. Mustafa, A. Mushtaq, T. Hayat and A. Alsaedi, Numerical study of MHD viscoelastic fluid flow with binary chemical reaction and Arrhenius activation energy, *Int. J. Chem. React. Eng.* 15 (2016) doi: [10.1515/ijcre-2016-0131](https://doi.org/10.1515/ijcre-2016-0131).
50. M. Mustafa, J. A. Khan, T. Hayat and A. Alsaedi, Buoyancy effects on MHD nano-fluid flow past a vertical surface with chemical reaction and activation energy, *Int. J. Heat & Mass Transf.* 108 (2017) 1340-1346.
51. L. F. Shampine, M. W. Reichelt and J. Kierzenka, Solving boundary value problems for ordinary differential equations in MATLAB with bvp4c; <https://www.mathworks.com/help/matlab/ref/bvp4c.html>
52. Solving boundary value problems for ordinary differential equations in MATLAB with bvp4c, *Tutorial Notes* (2007) 437-438.
53. M. Rahman and H. I. Andersson, On heat transfer in Bödewadt flow, *Int. J. Heat & Mass Transf.* 112 (2017) 1057-1061.